



Strategies for stable water splitting via protected photoelectrodes

Bae, Dowon; Seger, Brian; Vesborg, Peter Christian Kjærgaard; Hansen, Ole; Chorkendorff, Ib

Published in:
Chemical Society Reviews

Link to article, DOI:
[10.1039/c6cs00918b](https://doi.org/10.1039/c6cs00918b)

Publication date:
2017

Document Version
Peer reviewed version

[Link back to DTU Orbit](#)

Citation (APA):
Bae, D., Seger, B., Vesborg, P. C. K., Hansen, O., & Chorkendorff, I. (2017). Strategies for stable water splitting via protected photoelectrodes. *Chemical Society Reviews*, 46(7), 1933-1954.
<https://doi.org/10.1039/c6cs00918b>

General rights

Copyright and moral rights for the publications made accessible in the public portal are retained by the authors and/or other copyright owners and it is a condition of accessing publications that users recognise and abide by the legal requirements associated with these rights.

- Users may download and print one copy of any publication from the public portal for the purpose of private study or research.
- You may not further distribute the material or use it for any profit-making activity or commercial gain
- You may freely distribute the URL identifying the publication in the public portal

If you believe that this document breaches copyright please contact us providing details, and we will remove access to the work immediately and investigate your claim.

Strategies for stable water splitting via protected photoelectrodes

Dowon Bae,^a Brian Seger,^a Peter C.K. Vesborg,^a Ole Hansen,^b and Ib Chorkendorff^{a*}

^aDepartment of Physics, Technical University of Denmark, DK-2800 Kgs. Lyngby, Denmark

^bDepartment of Micro- and Nanotechnology, Technical University of Denmark, DK-2800 Kgs. Lyngby, Denmark

*Corresponding author: ibchork@fysik.dtu.dk; Tel: +45) 45 25 31 70; Fax: +45) 45 93 23 99

ABSTRACT

Photoelectrochemical (PEC) solar-fuel conversion is a promising approach to provide clean and storable-fuel (e.g., hydrogen and methanol) directly from sunlight, water and CO₂. However, major challenges still have to be overcome before commercialization can be achieved. One of the largest barriers to overcome is to achieve a stable PEC reaction in either strongly basic or acidic electrolytes *without* degradation of the semiconductor photoelectrodes. In this work, we discuss fundamental aspects of protection strategies for achieving stable solid/liquid interfaces. We then analyse the charge transfer mechanism through the protection layers for both photoanodes and photocathodes. In addition, we review protection layer approaches and their stabilities for a wide variety of experimental photoelectrodes for water reduction. Finally, we discuss key aspects which should be addressed in continued work on realizing the stable and practical PEC solar water splitting systems.

1. Introduction

Photoelectrochemical (PEC) water splitting is a promising approach to provide clean and storable chemical fuel (e.g. hydrogen) directly from sunlight, whereas photovoltaic (PV) solar cell technology directly converts solar energy into electricity, which must be consumed immediately or converted to a storable form of energy (e.g., using batteries or capacitors (with limited storage capacity)). The overall PEC water splitting process consists of three parts: (i) light absorption resulting in charge carrier generation, (ii) transportation of charge to the surfaces, and (iii) the utilization of excited photo carriers to drive catalytic reactions at the surfaces.^{1–3} Thus it is essential to transport the photo-generated carriers from a photo-absorber to a solid/liquid interface, where catalytic sites can oxidise or reduce the water. The reductive reaction leads to chemical fuel production, i.e., the hydrogen (H_2) evolution reaction (HER) from H^+ (in acid) or H_2O (in base), whereas the oxidative half-reaction produces O_2 from H_2O (in acid) or OH^- (in base) (oxygen evolution reaction – OER).^{3,4} The products of the overall reaction may be formed in a single compartment, *via* suspensions of photocatalyst particles,^{5,6} resulting in a system that produces a mixture of chemical products which subsequently should be collected separately to mitigate back reactions.⁵ Alternatively, both oxidation (at the photoanode) and reduction reactions (at the photocathode) can be carried out in separate compartments, such as on wired⁷ or on monolithic photoelectrodes;⁸ which eliminates the need for a separate gas separation step. However, this approach often requires high ionic strength to minimize Ohmic losses and localized pH gradient overpotentials (η)⁹ while minimizing product-crossover. Thus it is likely that either strong acid (low pH) or alkaline (high pH) conditions are necessary,^{9,10} but such harsh conditions may potentially lead to corrosion of the photoabsorber materials. This work will thus focus on analysing how to protect these photoelectrodes in separate compartments.

To date, there has been tremendous effort put into demonstrating efficient and chemically stable photoelectrodes for both HER and OER at various pH levels. By characterizing photoanodes and photocathodes independently, the expected performance of an integrated system without an external bias voltage can be directly estimated. The intersection of the overlapped linear sweeping voltammetry (LSV) or cyclic voltammetry (CV) data (see Fig. 1a) for each photocathode/anode indicates the maximum operating current density (J_{OP}) for the overall water splitting system. Metal oxides are materials that are often stable under water oxidation conditions, and typically provide the necessary band bending to allow a charge separation for

efficient photo-generated carrier transport in contact with the electrolyte. However, the optical transitions for many of the materials with optimal band gaps for water splitting are usually forbidden d-d transitions, and thus they have very small optical absorption coefficients.¹¹ In addition, carriers in metal oxide semiconductor d-bands are known to have poor mobilities, resulting in very short carrier diffusion lengths,^{11,12} which remain a major obstacle to achieve a high solar-to-hydrogen efficiency (STH%). As shown in Fig. 1, simple combinations of previously demonstrated LSV curves^{2,13–24} from the state-of-the-art photoelectrodes are still inadequate to form any highly efficient tandem water splitting system. In contrast, a combination of experimental low band-gap (E_g) photocathodes with a modelled ideal half-cell²⁵ with E_g of 1.8 eV results in J_{OP} above 17 mA cm^{-2} which corresponds to solar-to-hydrogen efficiency (STH%) above 20% (Note that J_{OP} values were estimated without considering Ohmic-loss between the two photoelectrodes and parasitic optical loss caused by the high E_g top-cell semiconductor). For instance, a BiVO_4 -based water splitting device combined with multi-junction a-Si PV cell has shown only a modest efficiency (4.9%)²⁶ due to low photocurrent output from the BiVO_4 photoanode layer. An earth-abundant low-cost iron-oxide (hematite, $\alpha\text{-Fe}_2\text{O}_3$) based photoanode coupled with perovskite solar cell has demonstrated barely above 4 mA cm^{-2} under alkaline condition.²⁷ The opposite case of high E_g photocathodes^{16,18,19} with low E_g photoanodes^{14,21,24} (Fig. 1b) shows essentially the same picture: The only pair of experimentally demonstrated photoelectrodes which results in a meaningful J_{OP} ($\sim 1.4 \text{ mA cm}^{-2}$) is a nanowire p-GaP-based photocathode¹⁹ in combination with a buried np⁺-junction GaAs-based photoanode.¹⁴ Both figures (1a and 1b) indicate that use of proven high-performance solar cell materials with charge-separation structures (*e.g.*, a buried junction), and appropriate corresponding protective materials are essential, in order to obtain a true practical and simple tandem PEC water splitting system for solar-fuel generation. Recent progress in nitrogen-doped BiVO_4 with the band-gap reduced by 0.2 eV over the pure BiVO_4 ,²² brightened the prospects for practical application to PEC water splitting, but it still has a large band-gap ($\sim 2.27 \text{ eV}$), which means it will never exceed above 10 mA cm^{-2} , indicating that oxides materials with lower E_g and reasonable photovoltage should be investigated.

This review covers the fundamental aspects of protection strategies for tandem PEC water splitting devices, focusing on inorganic thin film materials. First, we review strategies for protecting photoelectrodes, particularly for devices with buried-junctions, and the photo-excited carriers transport mechanisms across photoelectrode/electrolyte interfaces through the protection layers upon PEC water splitting reaction (*i.e.*,

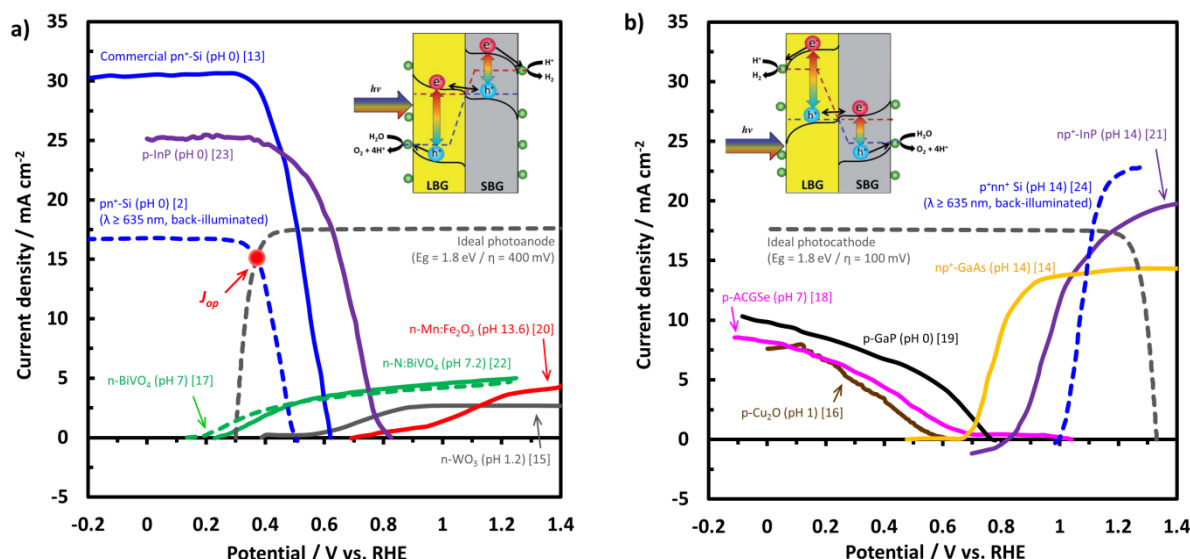


Figure 1. Overlaid current density-potential (J - V) behaviors for state-of-the-art half cells: Combination of small E_g (SBG in inset) photocathodes with large E_g (LBG in inset) photoanodes (a), and for the case of LBG photocathodes with SBG photoanodes (b). Schematic drawings for tandem water splitting devices for each case are illustrated as inset. The drawings were reproduced with permission from Ref. [10], Copyright 2014 The Royal Society of Chemistry. Modelled J - V curve for photoanode and photocathode (dashed dark grey) are projected to estimate theoretical maximum J_{op} of the overall water splitting system. Note that modelled J - V curve for the ideal photoelectrode was drawn using web-based simulation program.²⁵ Details of overlayers and catalysts can be found in Ref. [2,13–14].

HER and OER) are described. Secondly, we review various approaches (from the literature) for protecting photoelectrodes and how they impact stability and PEC performance. Finally, key aspects which should be addressed for practical tandem PEC water splitting system are given, along with technical remarks.

2. Background of protection strategies

2.1. Origin of semiconductor instability

Whether the semiconductor is stable under PEC condition depends on the alignment of the material's self-reduction potential (Φ_{red}) relative to $E(H_2/H_2O)$ for the photocathode, and the material's self-oxidation potential (Φ_{ox}) relative to $E(O_2/H_2O)$ for the photoanode, as described in early research by Allen Bard and others.^{28–30} A material is thermodynamically unstable when the Φ_{red} and Φ_{ox} are placed below or above of $E(H_2/H_2O)$ and $E(O_2/H_2O)$, respectively (Fig. 2a, b). Alternatively, when Φ_{red} is placed between the conduction band (CB) and $E(H_2/H_2O)$ under HER, the material stability depends on the relative split between the electron consumption rates for material reduction and for HER (k_{HER}), which is also called the branching ratio. Similarly, the oxidation reaction competes with consumption rates of photo-generated carriers for water oxidation (k_{OER}). Most photoelectrodes with relatively high photocurrents, such as Si, III-V and chalcopyrite semiconductors etc., are prone to be corroded quickly when in contact with an electrolyte of high ionic strength and, in general, these materials have a very narrow window of stability based on Pourbaix diagrams.^{29,31,32} The photocorrosion

of the material can be reduced by the use of relevant catalysts which improves charge transfer kinetics (*i.e.*, k_{HER} or k_{OER}) at the solid/liquid interface, and consequently reduce the surface oxidation.^{31–33} However, this strategy cannot prevent photoelectrodes from degradation during night time, where the materials do not have the benefits of photovoltage to provide a stabilizing anodic or cathodic bias.³⁴ Kinetic enhancement *via* morphology modifications can also be an approach for improving the stability of photoelectrodes. For instance, non-planar geometries, such as a rod or pillar array can reduce the distance that minority carriers must travel, and thus the charge transfer kinetics can be significantly improved as shown in previous studies.^{3,19} However, this approach also has the fundamental issue that it does not resolve the problem of degradation in the dark. In the case of Si – one of the most frequently used photoelectrodes, a Si surface exposed to an acidic electrolyte deactivates by forming oxide or silicic acid, *i.e.* SiO_2 and H_2SiO_3 etc., whereas it decomposes into $\text{H}_2\text{SiO}_4^{2-}$ under strong alkaline condition.³³ III-V semiconductors (GaAs, GaInP₂ and others) - photo-absorber materials for the most efficient solar-to-hydrogen conversion efficiencies (STH%) reported so far (>14%),²⁶ are also prone to chemical decomposition in strong acid where they form Ga^{3+} species, but this process takes place much more slowly.³⁵ Using metal-oxides with high *intrinsic* chemical stability is also a widely used strategy, however, as described earlier, relatively low PEC performance of those metal-oxides restrict their application in practical water splitting system.

We now turn to the use of high performance non-oxide materials with, *e.g.* Si. Si has a suitable E_g (1.12 eV) for the bottom cell of a tandem water splitting device, and is technologically mature despite the fact it has an indirect band gap and thus at least a 50- μm -thick absorber is needed in order to achieve substantial optical absorption.² Since Bockris *et al.* demonstrated a meaningful stability report using a crystalline n-Si photoanode protected by a Pt thin film under strongly acidic (pH 0) conditions for water oxidation (*i.e.*, OER) in 1984,³⁶ several protected Si devices with metallic protective catalyst films, including Ni (for OER)³⁷ and Ti (for HER)³⁸ have been demonstrated. However, losses due to parasitic light absorption by metallic layers causes a problem when this strategy is applied for the front-cell in a tandem device structure. Alternatively, metal-oxide semiconductors have been successfully used as protection layers for PEC electrodes owing to relatively high *intrinsic* chemical stability and minimal parasitic light absorption.

In light of the aforementioned approaches, using a protection layer with a high chemical stability for efficient photoactive semiconductors may provide an appropriate strategy to secure stable water splitting reaction of

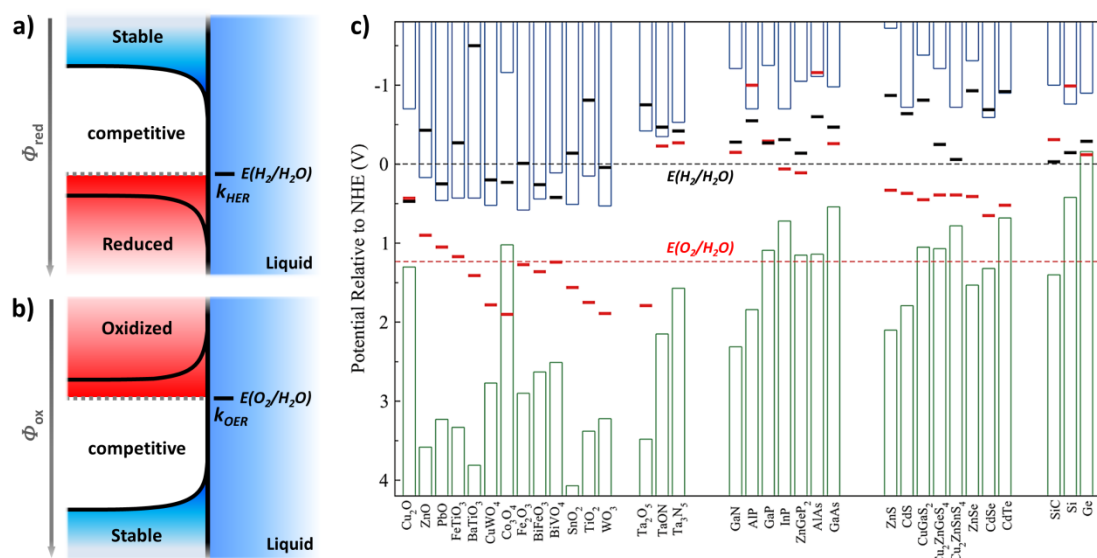


Figure 2. Stability change of the photocathode (a) as its reduction potential Φ_{red} shifts down from above the CB of p-type semiconductor to below $E(H_2/H_2O)$. Similarly for the photoanode case (b), stability of n-type material changes as its oxidation potential Φ_{ox} increases. Note that the illustration is not to scale. (c) Calculated reduction potential Φ_{red} (black bars) and oxidation potential Φ_{ox} (red bars) relative to the NHE and vacuum level for a series of semiconductors in solution at pH = 0, the ambient temperature 298.15 K, and pressure 1 bar. Figure (c) is reprinted with permission from [29]. Copyright (2012) American Chemical Society.

PEC electrodes. When the protection layer material has a Φ_{red} which is more negative than the CB of the photocathode, the system is thermodynamically stable under HER condition. Similarly, protective material with more positive Φ_{ox} than VB of the photoanode can be applied for the OER case. For instance, TiO_2 has very negative Φ_{red} (relative to RHE) compared to the HER potential²⁹ indicating that TiO_2 can be an effective protection material for photocathodes, as shown in Fig. 2c.

2.2. Protection strategies and charge transport mechanism

Since Kohl et al., demonstrated the first reliable HER and OER in 0.5M Na_2SO_4 (pH ~7) using TiO_2 protected photoelectrodes in 1977,³⁹ stable kinetics for various photoelectrodes with metal-oxide protection layer have been identified. Paracchino et al. coated a p- Cu_2O /n-Al:ZnO photocathode with a thin TiO_2 (~10 nm) film which shows quite stable PEC activity at relatively lower pH (~5).⁴⁰ Starting from this work, Lee et al. demonstrated stable HER using TiO_2 protected p-InP at pH 0.⁴¹ Chorkendorff and co-workers have also shown stable HER operation using a buried junction crystalline Si (c-Si) for both in strongly acidic (1M $HClO_4$)^{42,43} and strongly alkaline electrolytes (1M KOH).³⁴ For the photoanode case, McIntyre and co-workers have demonstrated stable OER both in strong acid (pH 0) and alkaline (pH 14) using TiO_2 /Ir protected c-Si with a metal-insulator-semiconductor charge separation junction which showed a photovoltage (V_{ph}) of 550 mV.⁴⁴ Lewis and co-workers have shown outstanding stability of 2200 hours (> 90 days) using TiO_2 /Ni protected buried np⁺-junction c-Si⁴⁵ and GaAs¹⁴ under OER condition in 1M KOH (pH 14). Studies have shown that multiple

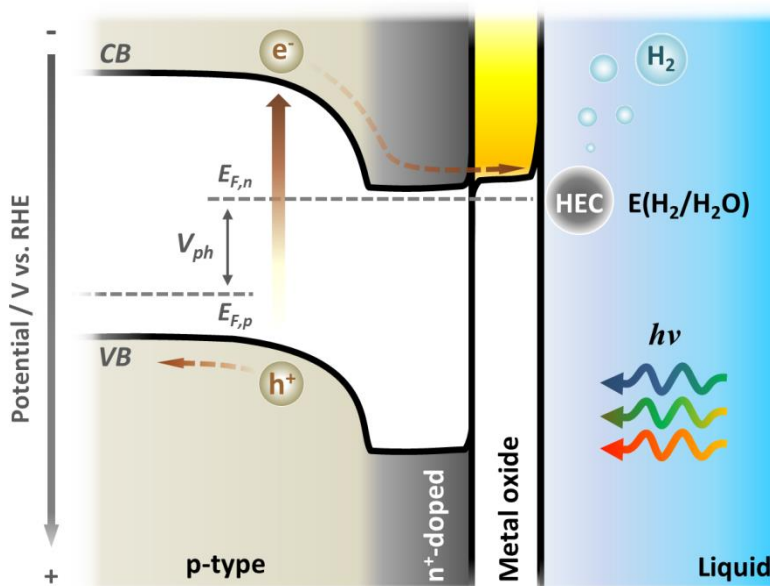


Figure 3. A schematic illustration of the band diagram of a photocathode with a buried pn^+ -junction protected by a n-type metallic oxide passivation layer. HEC stands for the hydrogen evolution catalyst, and $E_{F,n}$ and $E_{F,p}$ stand for the quasi-Fermi level for the electron and hole, respectively, the difference of which gives the photovoltage (V_{ph}) under illumination.

properties of the protection layer should be optimized for efficient charge transport under PEC conditions, including, but not limited to conductivity type, and band bending across the thickness. In general, metal oxide layers with n-type conductivity have been investigated as cathodic protection layers for HER.^{16,40,43,46} It has been widely accepted that electrons separated by a buried junction migrate to solid/liquid interface through the CB of n-type protection materials,^{2,13,40,43,46,47} as shown in Fig. 3.

Inversely, metal oxide layers with p-type conductivity coupled with photoanodes can transport holes via VB of the protection layer to the solid/liquid interface for OER (see Fig. 4a). In case of very thin (less than 2 nm thick) oxide insulators, such as SiO_2 and Al_2O_3 , direct *tunnelling* of charge carriers across the protection layers have also been reported,^{43,48} as illustrated in Fig. 4b. Interestingly, Hu et al.¹⁴ reported that a thick amorphous TiO_2 protection layer is applicable for the protection of photoanodes for OER due to hole transport through the bulk and a surface barrier of a “leaky” TiO_2 owing to defects in the bulk of the protection layer, which is also known as a *state-mediated transport* (see also Fig. 4c), as introduced by Campet et al. in 1989.⁴⁹ In the case of highly-doped n-type protection layer for photoanodes, electrons created by the OER reaction are injected into the CB of the protection layer and transported inwards toward the underlying photoabsorber. The electrons in the protection layer’s CB then recombine with holes at the interface between the photoanode and the protection layer. The holes to recombine with electrons from the CB of the protection layer are the photogenerated holes transported through the VB of photoabsorber (which is aligned with the CB of the

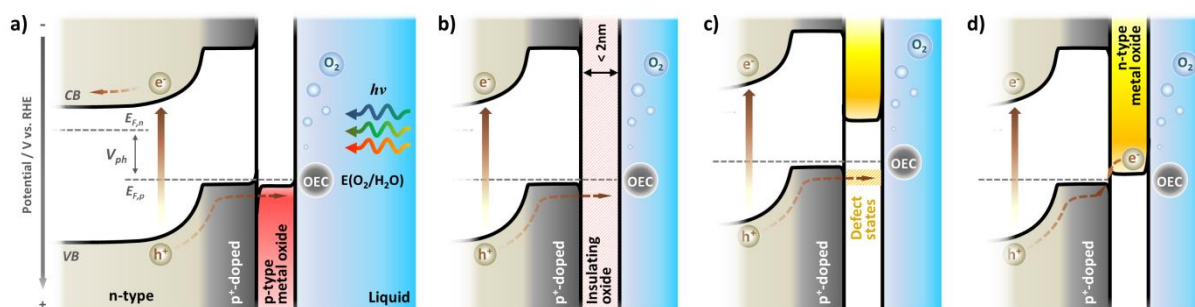


Figure 4. Illustration of band diagrams for protected buried np^+ -junction photoanode with various charge transport mechanisms: a) hole-transport via VB of p-type protection layer; b) hole-tunneling through the thin insulating oxide; c) hole-injection via state-mediate transport; d) electron consumption by recombination at the interface between the photoanode and n-type protection layer. Note that OECs stands for oxygen evolution catalyst.

protection layer (see Fig. 4d)), as shown by Mei et al. using c-Si and TiO_2 .⁵⁰ In other words, this form of photoanode protection layer transports *electrons in* – instead transporting *holes out*. Besides the above mentioned TiO_2 and other insulating oxides, various types of transition metal oxides, including NiO_x and CoO_x , have shown to be applicable depending on the operating condition and chemical reaction type. Further details for each case will be reviewed in the following sections.

3. Protection of photocathodes

Early experiments in solar-assisted hydrogen evolution emphasized the use of low band-gap solar cell materials, such as p-type Si⁵¹ and InP,^{52,53} by having HER catalyst (e.g. Pt⁵¹ and Rh⁵³) at the surface of those semiconductors. In these early studies of PEC electrodes for HER reaction, not much effort was devoted to protection of semiconductor surface from degradation, because those photocathodes materials were covered by oxide phase, such as SiO_2 , which is formed during cathodic reaction under oxygen contamination, or they have very slow decomposition reaction kinetics in such conditions. However, this kind of self-oxidation cannot be categorized as a protection layer in regard to the negative effect, *i.e.*, that oxidized surface hinders efficient charge transport leading to deactivation of the photoelectrode.

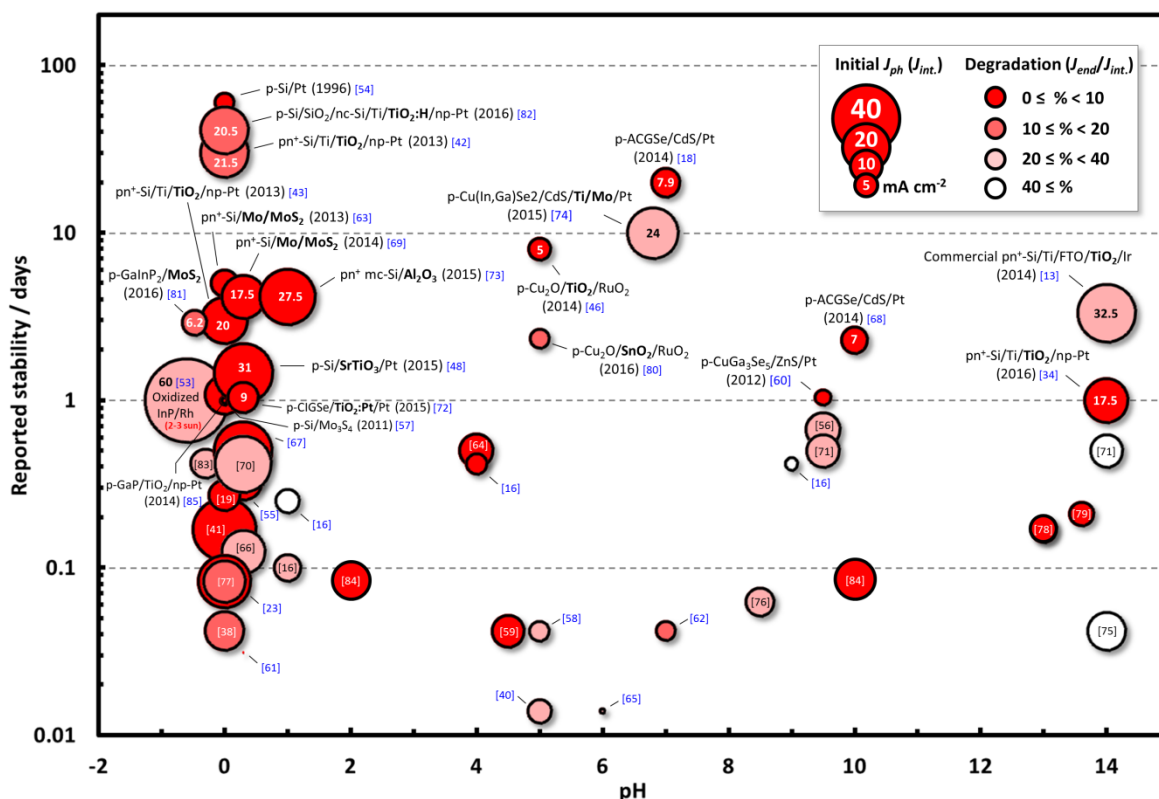


Figure 5. Chart visualizing data on reported stabilities of photocathodes for HER, versus tested pH condition, with resulting photocurrent and degradation rate indicated. Device structures for photocathode with reported stability longer than a day are noted. $J_{int.}$ is the initial photocurrent at the start of the stability test. Degradation rates are calculated using the ratio of the measured photocurrent at the end of the stability test (J_{end}) to $J_{int.}$. Detailed information on device structures and working conditions also can be found in Table S1 in ESI†.

Figure 5 summarizes the reported stability for many HER photocathode materials plotted against the pH level during the test. Note that for reported stabilities of overall water splitting from tandem or multi-junction devices the origin of degradation (HER or OER part) cannot be specified. Experimental details and device structures of the collected data from refs.^{13,16,18,19,23,34,38,40–43,46,48,53–85} in Figure 5 can be found in Table S1 in ESI†. As shown in Figure 5, most stability studies on HER are done in acid condition, particularly near pH 0, because many photoabsorber semiconductors are relatively stable under such conditions as stated previously. Notwithstanding of this nature of photocathode semiconductors, the importance of having long-term stable HER kinetics has to be emphasized. Since Maier et al. demonstrated 60 days long-term HER at pH 0 using p-type c-Si coupled with a photo-electrochemically deposited Pt layer,⁵⁴ various type of metallic layers have been applied as a protective HER catalysts. However, these metallic layers often limit efficient photocurrent output, even though they can isolate the photo-absorber effectively from the corrosive electrolyte, due to parasitic light absorption/reflection of the metallic elements. Nevertheless, they can be used for bottom cell applications, as described previously. Photocurrent output of most of the metallic HEC (hydrogen evolution

catalyst) coated c-Si based photoelectrodes ($\sim 10 \text{ mA cm}^{-2}$)^{53,59} are far from both the theoretical limit as well as experimentally obtained values from commercial c-Si PV cells, which exceeds 40 mA cm^{-2} under full AM1.5G illumination.^{2,86}

Transparent metal oxides are widely used as protection layers of photocathode materials. As described in the previous section, many metallic oxides are stable under water reducing conditions.³³ In addition, the relatively high intrinsic chemical stability of these metal-oxide semiconductors under dark condition³⁴ paves the way for the practical application in PEC water splitting devices. Furthermore, some metal oxides, such as TiO_2 , which has band-gap of around 3.2 eV,^{50,87} provide excellent optical transmittance in visible light region. Alternatively, thin metallic oxide insulators, such as SiO_x and Al_2O_3 , can be used as a protection layer. Depending on the semiconductor type and reducing condition, these insulating layers can be formed naturally when the photocathode material has direct contact with the electrolyte. In 1982, Heller et al. reported the formation of a thin 'native' oxide on p-InP surface by a 16 hours exposure to humid air,⁵³ which allowed for a quite stable PEC hydrogen production for a 24 hours. In an attempt to seek more uniform metal oxide formation approaches, several groups have reported use of an ultra-thin Al_2O_3 layer on p-Si,^{67,88} deposited using ALD (atomic layer deposition) which provides a compact layer with sub-nanometer (usually sub-angstrom) precision.⁸⁹ In various device designs, TiO_2 protected photocathodes are widely used over a wide pH range from acid to alkaline. Narrowing the pH range to near 0, Mo-based sulphides semiconductors (e.g., MoS_2) are also widely used as a protective HEC layer. The following sections discuss recent progress in stabilization of PEC hydrogen production, and both the limitations and prospects towards practical water splitting devices.

3.1. Metallic layers

Despite the parasitic light absorption issue, metals have been employed as protection layers for photocathodes without hindering charge transfer owing to their outstanding intrinsic conductive properties. Maier et al. demonstrated 60 days stable PEC hydrogen production using Pt coated p-type c-Si with 0.3 V of onset potential (V_{on}) in 1M HCl (pH 0).⁵⁴ Generally, noble metals are widely used as protection layers, but some non-noble metallic elements may also be used depending on working condition and device configuration. Moreover, the metals with a lower work-function than the photoabsorber, e.g., Ti with p-Si,⁹⁰ leads to a formation of a Schottky junction between the metal and semiconductor and introduces a built-in electric field, which promotes charge separation as shown in Fig. 6. In a recent report by Feng et al., a 5 nm Ti layer coupled

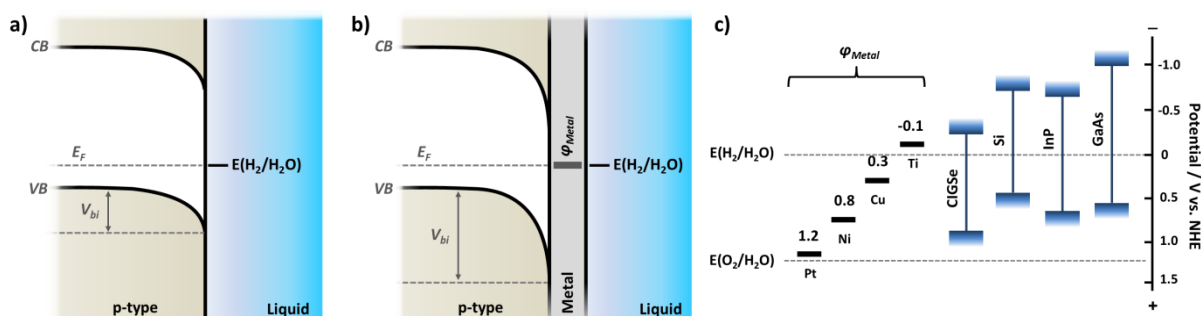


Figure 6. Proposed band diagrams for pristine p-type semiconductor (a) and metal-protected semiconductor with Schottky junction (b) in equilibrium with the $\text{H}_2/\text{H}_2\text{O}$ redox couple in contact with electrolyte. V_{bi} stands for the built-in potential. Band positions of widely used non-oxide photoabsorbers with approximate work function (ϕ_{Metal}) of selected metals are also shown in (c). The potential values in (c) are reported in the literature^{29,90} and relative to NHE (normal hydrogen electrode).

with a 2 nm Ni catalytic layers showed a V_{on} around 0.3 V vs. RHE with quite stable HER under illumination for 12 hours in both in 1M KBi (pH 9.5) and 1M KOH (pH 14).⁹¹ A demerit of this approach is that there is generally a significant carrier recombination at the metal/semiconductor Schottky junction interface, which results in very limited photovoltages. Seger et al.³⁸ used a thin Ti protection layer for HER in 1M HClO_4 (pH 0) between a pn^+ -Si photoelectrode and MoS_x layer, which had V_{on} of 0.33 V vs. RHE (0.47 V with Pt) with a relatively high fill factor owing to the buried pn^+ -junction. Unlike the previously mentioned semiconductor/metal direct contact which forms a Schottky junction, the contact of a metallic layer with a highly-doped semiconductor surface shows an Ohmic behaviour.

Despite the simplicity of the fabrication process of the metal protection layer, its application has been limited due to parasitic light absorption/reflection by these metallic layers. However, there should be no issues with light absorption/reflection for the case of the bottom cell in a tandem device configuration, since protection layers only need to be transparent when the illuminated side and the reaction side are coincident.¹⁰ As shown in recent works by Bae et al.² and Urbain et al.,⁷⁸ HEC acts under a pure dark electrocatalytic condition when the light is incident from the opposite side, thus indicating that bottom cell photoelectrodes in tandem water splitting device can be protected using a metallic layer regardless of its thickness. Recently, Crespo-Quesada et al.⁷⁶ demonstrated quite stable photocurrent output ($\sim 7.7 \text{ mA cm}^{-2}$) under back-side illumination for 1.5 hours in 0.1M borate electrolyte (pH 8.5) using a organometallic halide perovskite-based device (FTO/PEDOT:PSS/ $\text{CH}_3\text{NH}_3\text{PbI}_3$ /PCBM) coupled with thick Ag and Field's Metal (FM; InBiSn alloy), indicating that even water-sensitive semiconductors, such as lead halide type perovskites, can be used for PEC purpose with an appropriate protection strategy.

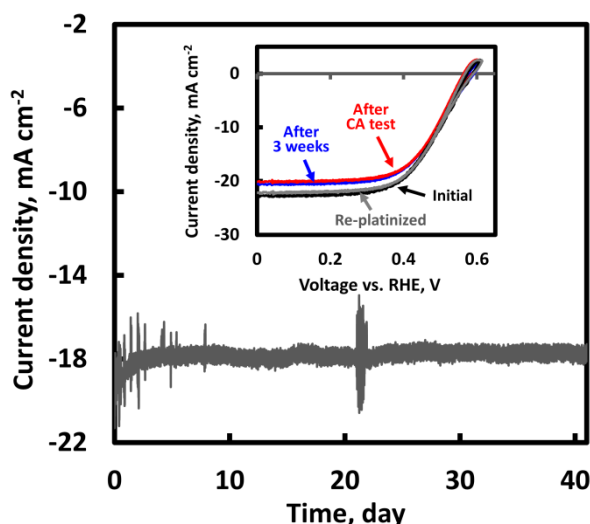


Figure 7. Long-term stability (chromoamperometry – CA) test of forming-gas (5% H₂/Ar) treated carrier-selective c-Si photocathode (c-Si/SiO_x/nc-Si at both front & back contacts) with 100-nm-thick sputtered TiO₂ protection layer. Photocurrent was measured at 0.4 V vs. RHE in 1M HClO₄ (pH 0). Initial CV prior to the CA measurement (black), CV after 3 weeks (blue), after 41 days (red), and CV from a re-platinized sample after the long-term CA test (grey) are shown in the inset. The figure is reprinted from ref. [82] with permission from Elsevier, Copyright 2016.

3.2. Metallic oxides

Many of the metal oxides are excellent protection layers for HER, however, as described in the previous section, TiO₂ is the most widely used protective metallic oxide material over the full pH range. At the same time, owing to its excellent optical transmittance ($E_g \geq 3.0$ eV)^{28,50} and good electron conductivity, most low band-gap photocathodes coupled with TiO₂ show relatively high photocurrent above 20 mA cm⁻² under illumination.^{23,41,43,82} Compared to other types of protection layers, TiO₂ protected photocathodes show relatively long-term stable operation with high photocurrent output. It has been shown that a TiO₂ protected c-Si (100) with a buried pn⁺-junction delivered a current density over 21 mA cm⁻² at 0.3 V vs. RHE with relatively low photocurrent loss (~14%) for 30 days under red-light (38.6 mW cm⁻²; $\lambda \geq 635$ nm) filtered, simulated sunlight.⁴² More recently, a TiO₂ protected MOS-based Si photocathode (c-Si/SiO_x/nc-Si) also delivered 41 days stable HER operation under the same PEC condition (Fig. 7),⁸² indicating that not only c-Si, but also chemically deposited thin-film Si can be successfully protected by TiO₂ under water reduction conditions in an acidic environment. The interfacing between the photoabsorber and protection layer is a critical factor for efficient charge transfer for high catalytic activity. The direct deposition of metal oxides may lead to surface oxidation of the photocathode (e.g. SiO_x) that builds an energy barrier which hinders photo-generated electron transport. A metallic and/or conducting interlayer applied between the metal oxide protection layer and photoanode can prevent the formation of an insulating layer during the subsequent deposition process. It has been shown that a thin Ti (5~10 nm) metallic interlayer can protect the Si surface

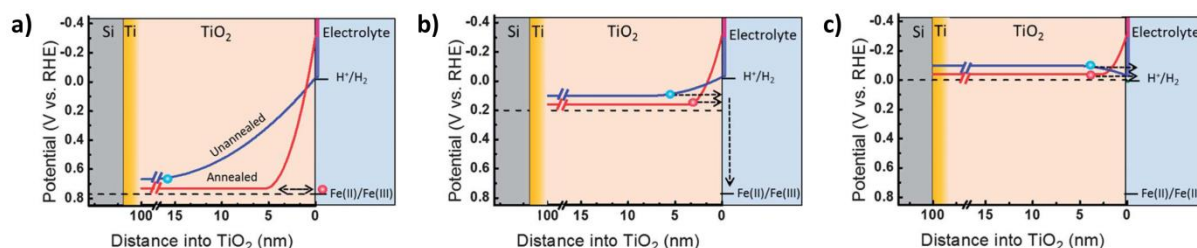


Figure 8. These band diagrams show the location of the TiO_2 conduction band of both the unannealed (blue lines) and vacuum annealed (red lines) samples as a function of depth into TiO_2 at the following electrochemical potentials: (A) +0.77 V, (B) +0.2 V and (C) 0.0 V vs. RHE. Note that the conduction band (CB) pinning at the TiO_2 /electrolyte interface. Electrons can tunnel through the TiO_2 only at the low potential range due to relatively wide depletion width, which hinders the efficient carrier transport. This figure was reproduced with permission from Ref. [47], Copyright 2013 The Royal Society of Chemistry.

against deactivation by sacrificial-oxidation of Ti interlayer at high temperature TiO_2 deposition process.^{2,13,34,43,50}

The doping level of the metal oxide layer is also a key parameter for efficient charge transport through oxide protection layer. High doping levels generally result in thin depletion layers, where tunnelling of the electrons at the CB of the oxide protection layer through the Schottky-barrier and at the oxide/liquid interface is possible. When the doping level is extremely high, this interface shows Ohmic-like behaviour as described earlier in chapter 2. In the case of TiO_2 , the doping level can easily be adjusted in an annealing process in vacuum which results in oxygen vacancies, and consequently increased dopant density. Seger et al.⁴⁷ revealed experimentally the importance of having a high doping level in the metal oxide protection layer by using photocathodes with two different doping levels. As shown in Figure 8, low-doped TiO_2 (unannealed) has a relatively long depletion width that electrons cannot tunnel through, while highly-doped TiO_2 (vacuum annealed) exhibits quite thin depletion width and with the donor density an order of magnitude higher than that of the unannealed film so that electrons can be injected to the electrolyte at lower potential than required for low-doped TiO_2 case. Similarly, Liang et al.⁷⁹ also demonstrated in their recent work that the H-doping via deposition of TiO_2 under H_2/Ar gas mixture flow can increase carrier density leading to enhancement of electron transport in TiO_2 films and a shorter depletion layer barrier.

In general, protective metal oxides, including TiO_2 , are poor HER catalyst, and thus coupling with a co-catalyst, such as Pt and Ru, is preferred for efficient HER kinetics. Taking into account parasitic light absorption of the metallic layer, a metal oxide protected photocathode coupled with thin covering co-catalyst film loses the merit of using metal-oxide protection layer. For this reason, catalysts in form of nanoparticles or small islands are preferred. Uniformly distributed Pt nanoparticles (~5 nm) formed on the TiO_2 surface by the

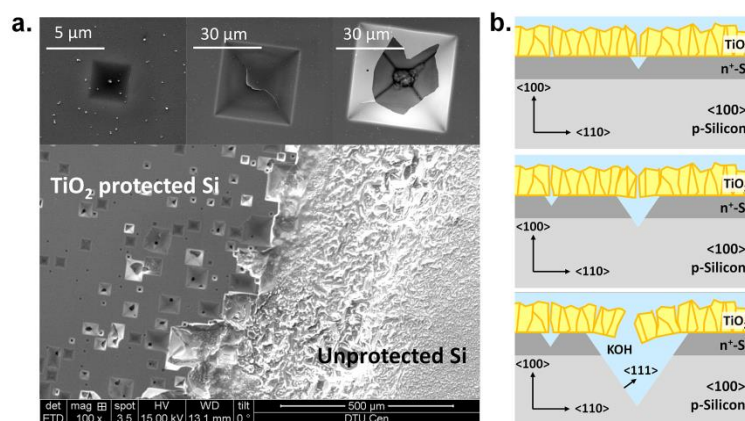


Figure 9. SEM images of a (100) oriented c-Si substrate with and without sputter deposited TiO₂ at 400 °C after immersion in an 1M KOH electrolyte (pH 14) for 3 days in the dark (a), and illustrations of the etch profiles of a (100) oriented Si through the pin-holes of TiO₂ protection layer during etching process in KOH solution. The figures were adapted from Ref. [34], copyright (2016) with permission from Elsevier.

(photo)electro-deposition method^{2,34,43,82} can support efficient catalytic HER and allow sufficient light transmission through the protective layer at the same time. However, this approach cannot prevent the simultaneous loss of Pt nanoparticles by the potential loss of TiO₂ during long-term experiments. To solve this problem, use of a mixed phase of TiO₂ and Pt (5%) has been demonstrated to protect a chalcopyrite photocathode (p-Cu(In,Ga)Se₂) under acidic conditions (0.5M H₂SO₄, pH ~0.3) in recent work by Azarpira et al.,⁹² where Pt particles are well distributed in bulk TiO₂ layer so that the photoelectrode could operate stable HER without significant degradation regardless of TiO₂ loss. It has also been demonstrated that earth-abundant catalysts, such as MoS_x, also can be applied as an additive for photocathode protection layer in acidic conditions. Bourgeteau et al.⁶¹ spin-coated mixed TiO₂ and MoS₃ nanoparticles and formed a thick TiO₂:MoS₃ protection layer (90 nm) onto a hetero-junction organic solar cell (ITO/PEDOT:PSS/P3HT:PCBM), which shows V_{on} above 0.5 V in low pH condition (0.5M H₂SO₄, pH 0.3). Although its photocurrent is quite low ($\sim 0.23 \text{ mA cm}^{-2}$ @ 0V vs. RHE), it is noteworthy that it was a first time demonstration of quite stable HER operation using an organic solar cell in such conditions under continuous illumination (45 min).

The use of an n-type Nb₂O₅ protection layer also deserves serious consideration since its protective property in acidic condition has also been shown,⁸⁵ using a planar type p-GaP/n-Nb₂O₅/np-Pt with a quite high V_{on} of 710 mV and stable photocurrent for 8 hours in 1M HClO₄. Despite of the subsequent slow degradation after the 8 hours, Nb-based metal oxide may prove to be one of the promising materials for protection of p-type materials, since it has a wide stability window in the Pourbaix diagram from pH 0.5 to 6.5.³³ Standing et al.¹⁹ also demonstrated V_{on} above 0.75 V with significantly increased photocurrent ($\sim 9 \text{ mA cm}^{-2}$ @ 0V vs. RHE) using nanowire (NW) Pt-coupled p-GaP, whose surface was chemically oxidized. Despite of this encouraging PEC

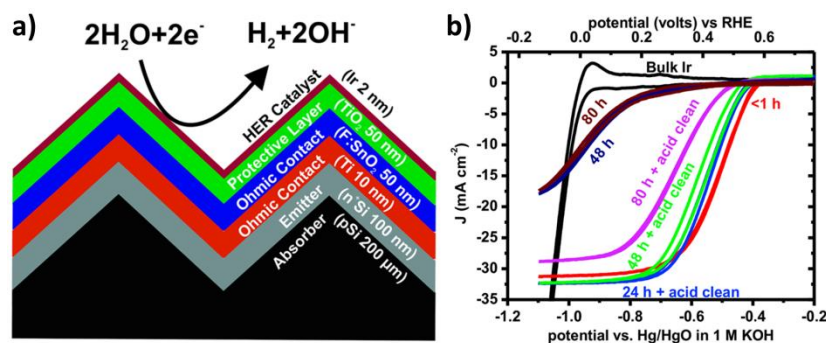


Figure 10. (a) Schematic of protected textured cells with catalyst and Ohmic-contact layers demonstrated in ref. [12]. Solution processed TiO_2 layer has been applied as a protection layer, and both Ti and FTO (F-doped tin oxide) are used as Ohmic-contact layers for efficient lateral charge transport. (b) J-V curves from CVs of photocathode after various times and treatments of stability testing at 300 mV vs. RHE (near maximum power point) in 1 M KOH (pH 14). The photocathode was then cleaned in acid (1 M HClO_4) via cycling from reducing to oxidizing potentials. Reprinted with permission from Ref. [12]. Copyright (2014) American Chemical Society.

activity, state-of-the-art PEC GaP's photovoltage lags behind the state-of-the-art GaP PV cell (1.56 V), thus there is still plenty of room for improvement.

Among the various metal oxide protected photocathodes with reported stability at mid-pH range, SnO_2 is noteworthy. Azevedo et al. demonstrated a SnO_2 (50 nm) protected p- Cu_2O photocathode in their recent work,⁸⁰ where the RuO_2 coupled photocathode showed a $V_{\text{on}} \sim 0.34$ V with quite stable cathodic photocurrent for more than 2.3 days at pH 5. In addition, a Cu_2O photocathode with ZnO/SnO_2 dual protection layer increased V_{on} (~ 0.55 V vs. RHE) and stability such that the system operated in the same conditions for 28 hours with only a relatively minimal in PEC activity.

However, unlike in acidic conditions, where the corrosion rate of the photocathode is generally slow due to self-limiting passivation of Si interface to SiO_2 ,³⁴ many photocathode semiconductors dissolve quite easily in alkaline electrolytes. When Si interacts with alkaline solution it corrodes via dissolution into SiO_4^- (rather than SiO_2). The wide stability window of TiO_2 in the Pourbaix diagram implies that TiO_2 can be applied in alkaline electrolyte as demonstrated in recent studies.^{34,79} Though irrespective of the 'intrinsic' stability of the TiO_2 semiconductor, the lack of a self-limiting passivation entails that the underlying Si will corrode continuously under any pinhole in protection layer, as shown in Figure 9. Kast et al.¹³ demonstrated the best performance c-Si based photocathode using a commercial textured pn^+ -Si solar cell device protected by complex multi-layer configuration of $\text{Ti}/\text{FTO}/\text{TiO}_2/\text{Ir}$ (10/50/50/2 nm). Ti and FTO layers were used as Ohmic-contact layers between a sprayed TiO_2 protection layer and a textured c-Si solar cell to provide a lateral electron pathway which can reduce the effect of locally deactivated regions by oxidation. As shown in Fig. 10, the sample showed significant decrease in activity after 2-days-operation, which was recovered after cleaning in acid. This

indicates that the degradation may be attributed to catalyst poisoning. However, an unrestored CV after the 3 days reveals physical damage on c-Si, which was proven by cross-sectional microscopic analysis. Bae et al. in Ref.³⁴ have also proved that p-type c-Si (100) can be protected for 24 hours in highly alkaline conditions (pH 14) using high power impulse magnetron sputtering (HiPIMS) that provides a TiO₂ protection layer with relatively high packing density, thus reducing pinhole density and the aforementioned issues accompanying them.

The fabrication method, in this sense, is of great importance. Conformal ALD coatings with outstanding step-coverage have also been applied for protection of photocathodes in alkaline media. Recently, a relatively thin (25 nm) ALD TiO₂ was deposited on a p-i-n a-SiC photocathode and PEC hydrogen production was performed in 1 M KOH (pH 14).⁷⁵ Unlike the previously mentioned cases in Refs.,^{13,34} ALD TiO₂ coated a-SiC shows a stable photocurrent for only 40 minutes, followed by a rapid deactivation, which leaves only 35% of the initial photocurrent after 1 hour. This was attributed mainly to uncovered pinholes in TiO₂ that exposed a-SiC to the highly corrosive electrolyte, which subsequently etched the a-SiC. This may be related closely with the fabrication conditions during protection layer deposition. Pinholes on the protection layer can be reduced or minimized by forming a dense and compact layer, but contamination, such as dust particles or debris adsorbed on the surface, cannot be removed simply by changing the deposition technique. Considering the fact that the above mentioned experiments were not carried out under the cleanroom conditions, much more stable PEC activities may be obtained if deposition is done in dust-free conditions. Deposition of metal oxide protection layer at larger thickness will certainly reduce pinhole density, however, thicker films will also increase series resistance and could additionally build a tunnelling barrier. The thickness-dependency of metal oxide resistance is noticeable, particularly, in the case of metallic oxides with low doping level. As shown in Fig. 8, a highly-doped metal oxide is required for efficient electron transfer across the TiO₂/electrolyte interface. Alternatively, the thickness of the protection layer should be thin enough to tunnel through (< 2nm) as described in chapter 2.2.

Except for the previously mentioned works of Heller et al. from the early 1980's,^{52,53} the protection property of several insulating metal oxide also have been verified recently. Al₂O₃ is a well reported insulator, which can protect photoelectrodes from corrosion in electrolytes, while photo-induced free carriers can tunnel through and then react with protons to produce hydrogen. Choi et al.⁶⁷ demonstrated a nanoporous (Np) Si photocathode protected by a thin Al₂O₃ (2.3 nm), which performed 12-hours-long stable cathodic current output in 0.5M H₂SO₄ (pH 0.3). An interesting feature is that the long-term stability test was performed at a

fixed negative potential at -0.3 V vs. RHE in pH 0.3, where Al_2O_3 is reduced to Al^+ . The stability of the Al_2O_3 protection layer after the long-term stability test is of doubtful, because Al is prone to be reduced and the Si surface tends to oxidize (*i.e.*, SiO_x) in such conditions as demonstrated by Maier et al. and others.^{54,57,59} Ji et al.⁴⁸ demonstrated a metal-insulator-semiconductor (MIS) PEC cell, where a thin SrTiO_3 (STO) (1.6 nm) layer was used as a protective insulator, and very stable PEC activity ($> 31 \text{ mA cm}^{-2}$ @ 0V vs. Ag/AgCl under 1-sun) was performed with a Pt co-catalyst for 1.5 days. Interestingly, it has been claimed that electrons can be injected through the conduction-band of c-Si and through the MBE-grown STO on Si due to the small band offset between these two materials (see Fig. 11a inset). However, detailed description or calculation of the low band-offset at the c-Si/STO interface was not provided. Although Pt is an excellent HEC, its large work function is similar to that of p-Si, which cannot explain the photovoltage obtained in that work (~460 mV). Detailed calculation of the band alignment after equilibrium with H^+/H_2 reaction should be supported considering doping concentration and Fermi level of the STO layer to describe exact charge transport mechanism.

Beside the above described silicon and III-V based photocathodes, chalcopyrite-based thin film photocathode, *e.g.* p-type $\text{Ag}_x\text{Cu}_{1-x}\text{GaSe}_2$ (ACGSe), CuGaSe_2 (CGSe), $\text{Cu}(\text{In,Ga})\text{Se}_2$ (CIGSe), also have shown good HER stability, but mostly in weak acidic and alkaline media (Figure 5), because most chalcopyrite-based photocathodes are covered with a CdS layer,^{18,56,68} which is soluble in highly acidic and alkaline media. The CdS layer, which is n-type typically, plays a role as an electron transfer layer by forming pn-junction with the chalcopyrite layer, but not as a protection layer. Direct contact with a n-type TiO_2 protection layer typically struggles to provide an efficient charge separation as shown by Azarpira et al.⁷² On the other hand, Ros et al.⁷⁰ have coated a TiO_2 overlayer as a protection layer on a CIGSe/CdS/i-ZnO/AZO multilayer structure and demonstrated efficient photocurrent output ($> 40 \text{ mA cm}^{-2}$) with a relatively high V_{on} of 0.6 V vs. RHE in 0.5M H_2SO_4 (pH 0.3). Despite the recent progress in acidic electrolytes, continued work on protection property of TiO_2 for the chalcopyrite-based photocathodes in highly alkaline media is also needed, similar to the TiO_2 -protected silicon photocathode cases in highly alkaline media.^{13,34,79}

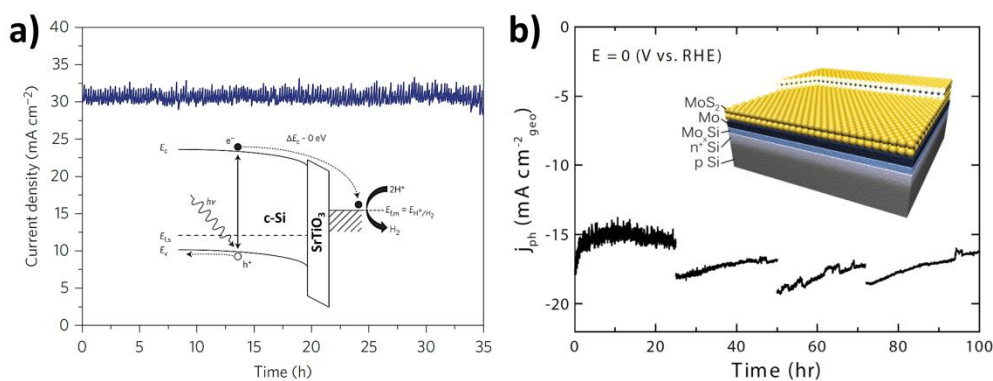


Figure 11. Stabilities as indicated by the steady-state photocurrent characterization with c-Si/STO/Ti/Pt (a) (Reprinted with permission from ref. [48] Copyright 2016 Nature Publishing Group) and pn⁺-Si/Mo/MoS₂ (b) (Adopted with permission from ref. [69] Copyright 2014 WILEY-VCH Verlag GmbH & Co. KGaA, Weinheim) held at 0 V vs. Ag/AgCl and RHE, respectively. Both tests were measured under 100 mW cm⁻² illumination in 0.5 M H₂SO₄ (pH 0.3). Schematic structures of the photocathode are also shown in inset.

3.3. Other layers

Other protection layer candidates include carbon⁶² and the MoS_x family^{16,61,63,66,69,77,81} of materials. In this section, we focus on the latter group since this has shown some success when applied as cathode protection layers. MoS₂ and some other di-chalcogenides have outstanding stability in strongly acidic electrolyte - even under above band-gap illumination. A recent study measured finite corrosion rates of MoS₂ edges, but only under extremely intense laser illumination (corresponding to 10⁷ times the solar irradiance), and only when the photon energy was above the band-gap, and only when oxygen was present.⁹³ In general though, MoS₂ is an extremely durable material in a cathodic environment in very strongly acid electrolytes as shown experimentally in some studies (also shown in Fig. 11b),^{63,69,81} but so far its use has been less widespread. Perhaps this is due to its two main disadvantages: i) limited conductivity perpendicular to the MoS₂ planes and ii) significant optical absorption. MoS₂ is a semiconductor with a band-gap in the red part of the spectrum such that optical absorption is an important consideration which means that the thickness of the MoS₂ film should be minimized in any design where the MoS₂-protected photocathode is facing the light source. If MoS₂ is used on the backside with respect to the illumination, optical absorption is of course a non-issue, as mentioned earlier.^{2,10} Another reason to limit the thickness of an MoS₂-based protection layer is that its electrical conductivity perpendicular to the 2D planes of MoS₂ - *i.e.* its conductivity through the protection layer out to the electrolyte - is low. This means that the use of a thick (*i.e.* 50 nm) MoS₂ layer for electrode protection of the underlying photoabsorber would probably result in unacceptable loss of photovoltage due to the series resistance imparted by the protection layer. However, heavy doing (or strongly cathodic conditions) could shift

the chemical potential enough to achieve much better electron transport, and we speculate that is why MoS₂ protection layers work, but a detailed mechanism has not been studied fully.

MoS₂ itself (if structured correctly) has the advantage of also being an excellent hydrogen evolution catalyst.^{94–}

⁹⁷ This offers the compelling prospective of combining the function of protecting the photoabsorber from corrosion in the electrolyte with the function of providing electrocatalytically active sites for HER in the same, non-noble material. In conclusion, a thin MoS₂ layer should be able to simultaneously achieve great chemical corrosion stability, moderate optical loss and Ohmic resistance, and comparatively good HER catalytic performance for a non-noble material in a concentrated acidic electrolyte.

In 2012, MoS₂ (including amorphous MoS_x⁹⁸) was used on a buried-junction (pn⁺-Si) silicon photocathode in conjunction with a metallic titanium protection layer.³⁸ This system showed promising performance, but its stability was erratic. Samples would run without apparent degradation on the order of a few hours (between 1 and 8 hours) before failing abruptly. The first use of MoS₂ as a protection layer on a photocathode to achieve multi-day stability was in 2013.⁶³ In this case, an MoS₂- (or WS₂) layer, grown by sputtering 10 nm Mo (or W) directly on a buried-junction (pn⁺-Si) silicon photocathodes was converted in a treatment with H₂S/H₂, and resulted in photocathodes where both protection and HER activation are derived from the resulting MoS₂- (or WS₂) layer.⁶³ While the WS₂-protected photoelectrodes showed less than 20 hours stability and low photovoltage, the MoS₂-protected photoelectrodes worked remarkably well and showed no degradation after operating for 5 days. Besides the MoS₂ protection and catalytic layer, a MoS_x overlayer was also tested as a co-catalyst.⁶³ Almost exactly the same protection approach was taken by another group the following year with the main difference being a thinner sputtered Mo layer (3.6 nm instead of 10 nm) and a correspondingly lower sulfurization temperature.⁶⁹ In this case, the durability was tested for 100 hours - again with no signs of degradation, and with similar photoelectrode performance. In addition to the MoS₂ protection layer, a Mo₃S₁₃²⁻ cluster co-catalyst was also investigated in this work.⁶⁹ Very recently the same group used the same method of sulfurizing a 3.6 nm sputtered Mo film to protect a p-GaInP₂ photocathode.⁸¹ In this case they achieved ~6 mA cm⁻² of photocurrent (partially due to an estimated 40% of the photons above the band-gap of GaInP₂ being absorbed in the MoS₂ film) and a stability of 60 hours followed by a decay, which they ascribe to pinholes in the protection layer.

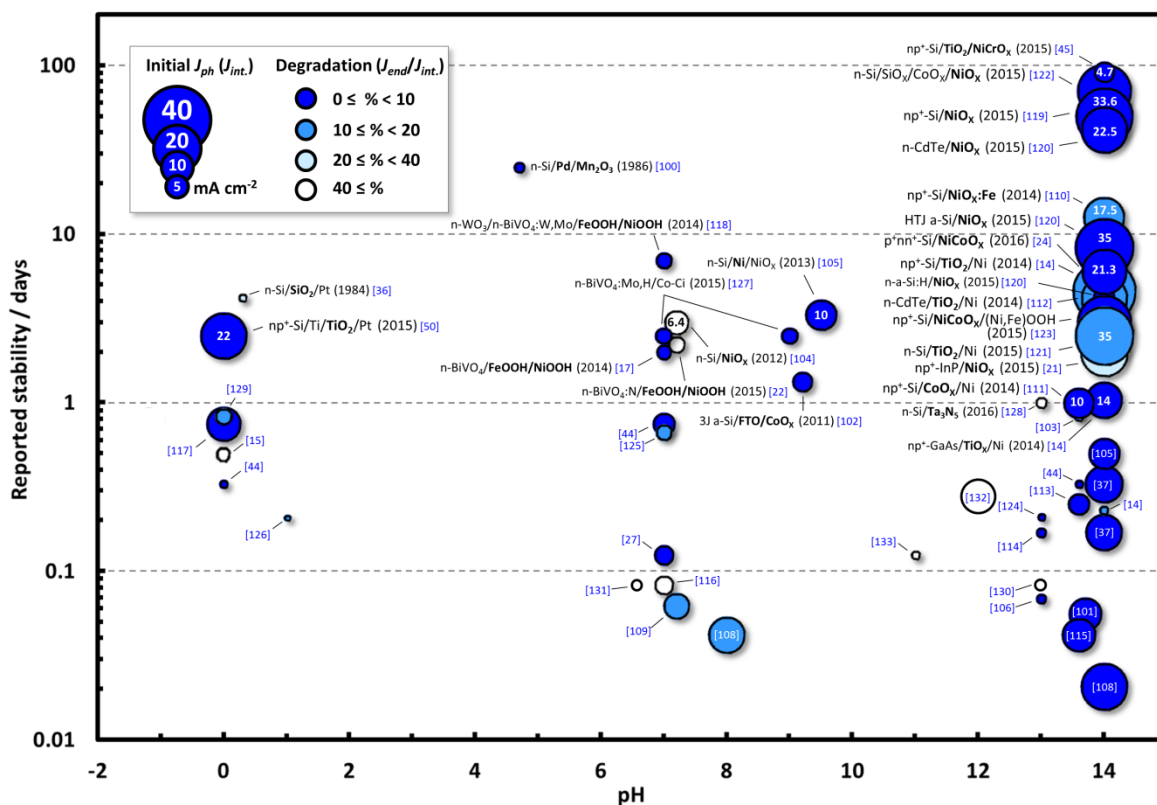


Figure 12. Chart visualizing data on reported stabilities of photocathodes for OER, versus pH of the test condition, illustrating photocurrent and degradation rate. Device structures for photoanode with reported stability longer than a day are noted. Detailed information on device structures working conditions also can be found in Table S2 in ESI†.

In a tandem water splitting device design where the photoanode is facing irradiation (top cell), the optical absorption of the cathodic protection layer is irrelevant as previously mentioned so the relevant questions are: can the stability be increased to 1000s of hours - *e.g.*, by the elimination of pinholes; and whether ultra-thin MoS₂ layers with low Ohmic resistance can be stable for such a long term operation. It seems that the obvious research direction would be to make conformal coatings of MoS₂ (for instance via ALD). While there are a large amount of oxides for protection layers that are currently being deposited with ALD,⁹⁹ to the best of our knowledge, there has yet to be tested an ALD-grown MoS₂ or other sulfide protection layer on a photoelectrode.

4. Protection of photoanodes

Since Contractor et al. reported a reliably stable PEC water oxidation reaction for more than 4 days using n-type c-Si coupled with Pt in 0.5M H₂SO₄ (pH 0.3),³⁶ a variety of photoelectrodes have been used to develop photoelectrochemically stable water oxidizing photoanode systems as a counter part to the photocathode for the water splitting reaction. Just as in the photocathode case, considerable efforts have been made, as shown in Fig. 12, where data were collected from Ref.^{14,15,17,21,22,24,27,36,37,44,44,45,50,100-133} While there are many excellent

HER catalysts (*e.g.*, Pt, MoS₂, CoP), in contrast, there is a serious struggle to find acceptable OER catalysts in acidic environments.⁹⁵ The majority of non-noble catalysts for OER suffer from deleterious degradation side reactions, particularly in the low pH region,¹³⁴ where the bleaching of the electrocatalyst and loss of OER kinetics results. Unprotected non-oxide photoanode materials, on the contrary, oxidize under OER conditions by forming an insulating layer that potentially prevents decomposition of semiconductors during OER reaction.⁴⁴ Only a few OER catalysts, including IrO_x and RuO_x, are proven to be stable under acidic OER conditions,^{117,135} and thus, significant attention has been devoted to protection of photoanodes in alkaline media as shown in Fig. 12.

Just as in the photocathode case shown in Fig. 5, TiO₂ has been widely used as an anodic protection layer. For instance, stable water oxidation reaction of TiO₂ protected c-Si simply coupled with metallic OER catalyst, such as Ni and Ir, were demonstrated in the pH range from 0 to 14.^{14,44,112} However, the charge transport mechanism is quite different from that of the cathodic protection case, where the photo-induced carriers generally are injected through the conduction band of the n-type metal oxide protection layer. Several recent works have claimed hole-transfer *via* state-mediated (defect-state) transport (see also Fig. 4c) through a thick metal oxide layer from the photoanodes,^{14,107} while a majority of the works claimed hole injection via tunnelling for ultra-thin metal oxide cases.^{36,44,124} The detailed case study will be discussed in this section focusing on thin film protection materials for stable OER activity.

However, above all, p-type metal oxides, including NiO_x and CoO_x, are most widely investigated, because they act as excellent hole-conducting protection layers, particularly in high pH conditions. This is because of their excellent hole-transfer and electron-blocking properties due to high CB edge positions.^{24,136–138} In addition, these transition metal oxides act as active OER catalysts by forming oxyhydroxides with higher oxidation states (*via* surface hydroxylation of the nickel or cobalt, *e.g.* NiOOH and CoOOH), which easily incorporate Fe during anodic reaction that reduces the overpotential for OER activity significantly.^{24,139,140} Thin metallic OER catalysts, including Ni and Co, will also be discussed. Owing to the relative simplicity of the fabrication process compared to metal oxide, the protection strategy using a metallic layer is also widely used. However, unlike the HER cases, where the metallic layers tend to be reduced to metallic ions under cathodic condition, at high potentials, metallic OER catalysts form oxides and/or oxyhydroxides which are OER active sites.^{105,114,141}

4.1. Metal

As opposed to the photocathode case for PEC hydrogen production in chapter 3.1, the metals with a higher work function than the photoanode semiconductor can form a built-in potential by introducing a Schottky-junction at the interface between the metal and the n-type semiconductor (see Fig. 6), which promotes separation and transport of the photo-induced charge carrier (holes in this case) to the electrolyte for water oxidation reaction.¹⁰⁵ Kenny et al. reported in Ref.¹⁰⁵ quite stable water oxidation performance using a 2-nm-thick Ni coating on n-type c-Si in both aqueous 1M KOH (pH 14) and K-borate + Li-borate electrolyte (pH 9.5) for more than 12 hours and 3 days, respectively. The key feature is formation of a MIS charge-separation structure by forming a native SiO₂ insulating layer between the n-type c-Si and Ni metallic layer that provides a relatively high photovoltage of ~500 mV. In addition, oxidized Ni species are formed at the Ni metal surface in contact with the electrolyte at oxidative potentials; they act as the OER active sites as mentioned earlier. Higher photovoltage is also obtainable without losing its PEC stability by adding a metal with high work function, such as Pt and Pd.^{101,100} Particularly, Kainthla et al.¹⁰⁰ demonstrated outstanding OER stability under illumination for more than 25 days using a Pd coated n-type c-Si coupled with Mn₂O₃ as a co-catalyst. Although it showed low photocurrent output (~1.4 mA cm⁻² @ 1.3V vs NHE), the relatively high photovoltage (~550 mV) performance is worthy of notice considering its publication time (1986) and relatively low pH condition (~4.5). As described in the previous section, most metallic protection layers form metal oxides or oxyhydroxides under OER conditions, and thus further details are discussed in following metal oxide chapter for conciseness.

4.2. Metal oxides

When dealing with semiconductor protection layers they need to conduct charge, typically holes, with minimal resistive barrier. The resistive barrier includes both bulk resistance and resistance at the semiconductor-electrolyte interface due to band bending.

NiO is a Mott-insulator, which means its band gap is primarily derived from a splitting between the d-orbitals. Thus both the VB and CB are a function of the temperature, and this makes NiO different from many other common oxides (TiO₂, WO₃, etc.) whose band gap are primarily derived from a VB based on the O2p orbital and a CB based on the metallic s-orbital. Since the VB of NiO is based on a d-orbital rather than the typical O2p orbital, it will typically be more reductive in potential. This is born out in experiments where NiO typically shows a valence band around 1.0 V vs. RHE¹³⁶ whereas oxides such as TiO₂ and WO₃ show a valence band near 3.0 V vs. RHE.⁸⁷

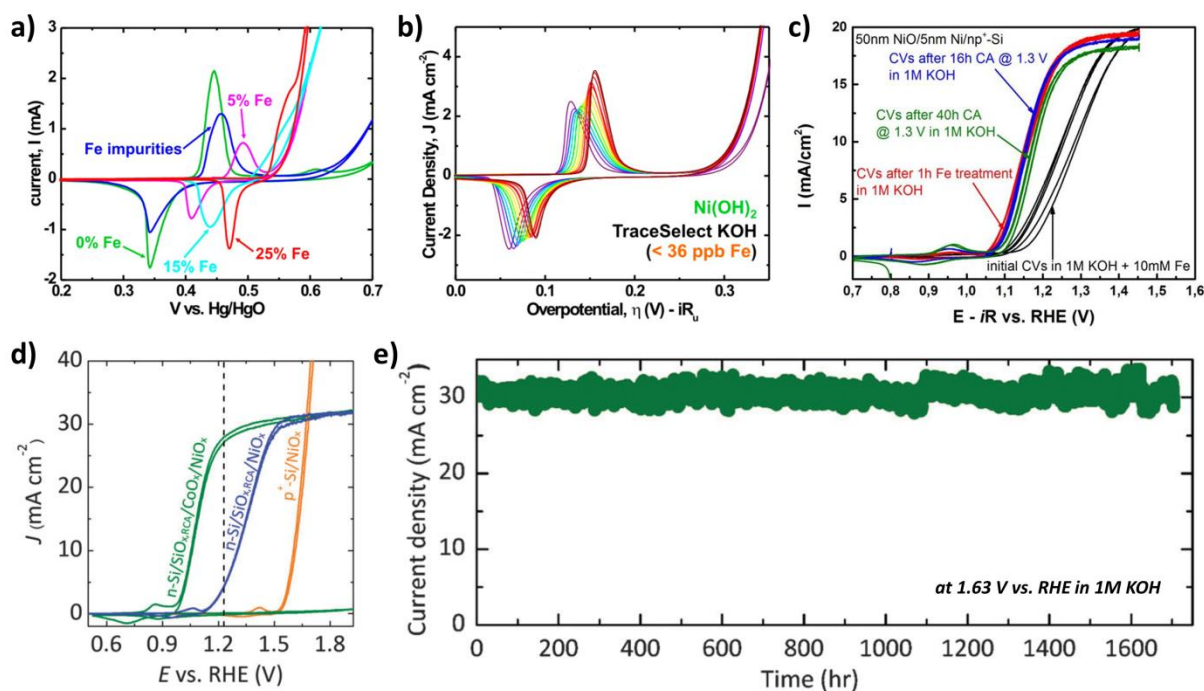


Figure 13. CV scans of $\text{Ni}_{1-x}\text{Fe}_x(\text{OH})_2/\text{Ni}_{1-x}\text{Fe}_x\text{OOH}$ films (a) and CV taken during 1 hour aging of $\text{Ni}(\text{OH})_2$ film (b) under dark condition in 1M KOH containing low-ppm Fe (< 36 ppm). Reproduced with permission from ref. [144]. Copyright 2014 American Chemical Society. (c) CV curves of PEC measurements of Fe-treated NiO thin films on $\text{np}^+\text{-Si}$ photoanodes after various treatments under 38.6 mW cm^{-2} ($\lambda \geq 635 \text{ nm}$). Reprinted with permission from the American Chemical Society (ref. [114]). (d) CVs of $\text{n-Si/SiO}_x/\text{CoO}_x/\text{NiO}_x$, $\text{n-Si/SiO}_x/\text{NiO}_x$, and n-Si/NiO_x and (e) chronoamperometry (CA) of $\text{n-Si/SiO}_x/\text{CoO}_x/\text{NiO}_x$ photoanodes measured at 1.63 V vs. RHE. Both experiments were carried under AM 1.5G solar illumination. Reprinted with permission from the ref. [122] Published by The Royal Society of Chemistry.

Since NiO naturally acts as a p-type semiconductor, this material typically transfers charge through its valence band. Since the VB is located at a potential more reductive than the actual O_2 evolution potential (thermodynamic potential + overpotential), there should be no resistance due to band bending since at these potentials there will actually be an accumulation layer or band de-pinning at the surface. However since NiO has a bulk resistance of $1.4 \times 10^{-4} \Omega \text{ cm}$,¹⁴² it can produce noticeable resistance if the thickness is significantly large.

However with a wide band gap of 3.4–3.7 eV,^{109,137,143} a NiO protection layer basically does not absorb visible light from solar irradiation, and correspondingly, thin Ni-based oxide layers (30–50 nm) show high optical transmittance above 90% in visible light region.^{104,110,119} In addition, NiO is quite stable in base, (though unstable in acid), and is also one of the best O_2 evolution catalysts if doped with Fe, as shown in Fig. 13a–c.^{110,139}

In 2012 Sun et al. started investigating NiO on n-Si for PEC devices.¹⁰⁴ In this work they used NiO for three purposes, a protection layer, an O_2 evolution catalyst (*via* forming NiOOH) and as a material to create band bending and hence photovoltage within the Si. Unfortunately, the onset potential for O_2 evolution was very

near the $\text{H}_2\text{O}/\text{O}_2$ redox potential and currents were tested only up to 1 mA cm^{-2} . The photovoltage provided by the n-Si/ NiO_x was found to be on the order of 300 mV under A.M 1.5 condition. The PEC experiments were done at neutral pH, and there was little in-depth work into its durability. Further work using a NiO/RuO_x on n-Si nanowires provided slightly better performance but showed significant degradation after 500 cycles.¹⁰⁹ While low in photocurrent and photovoltage, these initial works unveiled the great potential of using NiO as a protection layer.

In 2014 Mei et al. investigated a $\text{pn}^+\text{-Si}/\text{Ni}/\text{NiO}_x$ structure for use in PEC O_2 evolution in alkaline conditions (1M KOH).¹¹⁰ Unlike the previous approach by Sun et al.,¹⁰⁴ they used a built-in Si homojunction to create band bending within the Si. Since the NiO_x was sputter deposited, a thin Ni layer was pre-sputtered onto the Si before the NiO to prevent silicon oxidation. When NiOOH is used as an O_2 evolution catalyst (OEC), often times researchers allow very minute concentrations of Fe contaminants found naturally in their electrolyte (from impurities in NaOH or KOH) to intercalate into the NiOOH to form the highly active NiFeO_x catalyst (Fig. 13c). In Ref. [110], however, they intentionally pre-intercalated Fe into their electrode before actual O_2 evolution, which allowed them to achieve optimal performance directly from the beginning of their water splitting experiments. This approach allowed for an anodic photocurrent of 10 mA cm^{-2} at a potential of 1.15 V vs. RHE. Furthermore they showed this material to be stable in a basic environment for 2 weeks with only minimal signs of degradation. Through analysis of the electrolyte after 24 hours of testing, they determined (through inductively coupled plasma (ICP) analysis) that their NiO_x was corroding at a rate of between 0.06-0.08 monolayers per day, which corresponds to approximately 2,800 days or 7.6 years of continuous operation to fully corrode.

Very shortly after the Mei work, Sun et al. showed a very similar system and demonstrated stability for 50 days.¹¹⁹ They compared their NiO protection layer to a thin Ni metal layer, and showed that NiO acts as an anti-reflection layer in addition to a protection layer. Following the same approach NiO was shown also to work as an excellent protection layer for an InP photoelectrode comprising a $\text{np}^+\text{-InP}/\text{NiO}$ electrode.²¹ This device produced 10 mA cm^{-2} O_2 evolution current at a potential of 1.0 V vs. RHE and was shown to be stable for at least 48 hours.

While the work by Sun et al. that used a NiO to induce band bending in Si only produced ~300 mV of photovoltage, switching to CoO_x led to 560 mV photovoltage during O_2 evolution (and 640 mV photovoltage when using a ferrocene redox couple) (see also Fig. 13a).¹²² This work used only 2-3 nm of CoO_x to induce a

MIS-like charge separation by forming c-Si/SiO_x/CoO_x and they were still able to deposit a thick NiO layer (~85 nm) on top of it with no detrimental effects to its transparency or its ability to protect for more than 70 days under continuous light-illumination.

Besides the c-Si cases described above, recent studies have revealed that the protection strategy using Ni-based metal oxides can be applied effectively to various thin-film semiconductors, such as a-Si:H, CdTe¹²⁰ and Ta₃N₅.¹²⁸ Thin film metal-oxide photoanodes, particularly BiVO₄-based photoelectrodes also showed noticeable OER stability. Various oxyhydroxides, e.g. electrodeposited NiOOH and FeOOH,^{17,22,118,125} have been applied to the BiVO₄ as protecting OER catalysts, however, most of those studies are limited to neutral pH (Figure 12), mainly due to photoelectrochemical corrosion of the BiVO₄ in highly alkaline media.¹¹⁴ Lichterman et al.¹⁰⁶ demonstrated that a thin ALD CoO_x coated BiVO₄ shows significantly improved OER stability in 0.1M KOH (pH 13) indicating that the fabrication method is of great importance just as in the case of photocathode described above in the section 3.2.

Cobalt-based oxide materials are also a widely used protection layers for photoanodes with a quite high resistance to photocorrosion. Similar to Ni-based oxide materials, CoO_x is also known to be oxidized and form oxyhydroxides, for instance CoOOH, that easily incorporates Fe from the electrolyte easily.¹⁴⁰ Interestingly, time-dependent behaviour in OER activity varies with reports. Bae et al. and other group reported gradual decrease of OER activities of CoO_x (CoO, Co₂O₃, Co₃O₄ mixed phase) coupled c-Si photoanodes in their recent works,^{24,122} while Yang et al.¹¹¹ reported very stable OER activities under same condition (1M KOH, pH 14) using an np⁺-Si/CoO_x photoanode. In regards to this, several works on pure electrochemical stabilities of cobalt oxide can provide a clue to understand this discrepancy. Burke et al.¹⁴⁰ demonstrated a gradual enhancement of OER activity in KOH electrolyte due to the iron-incorporation in CoOOH formed by the electrodeposition method. Jiang et al.¹⁴⁴ also reported a quick decrease in overpotential for OER of the electrodeposited CoOOH for the first 2 min., followed by stable OER activity for more than 10 hours. Tung et al.¹⁴⁵ revealed in their recent work that Co₃O₄ tends to decompose gradually under water oxidation condition, whereas CoO supported Co₃O₄ showed very stable OER activity for 1,000 hours under the same condition, indicating that stability of CoO_x phase is related with volume expansion during the phase transformation to CoOOH.

While there has been great interest in using TiO₂ as a photoanodic protection layer since the 2014 work of Hu et al.,¹⁴ there has actually been some very significant works investigating TiO₂ in a photoanodic environment before the Hu work. In 1977 Tomkiewicz et al.¹⁴⁶ investigated the corrosion protection ability of TiO₂ on n-type

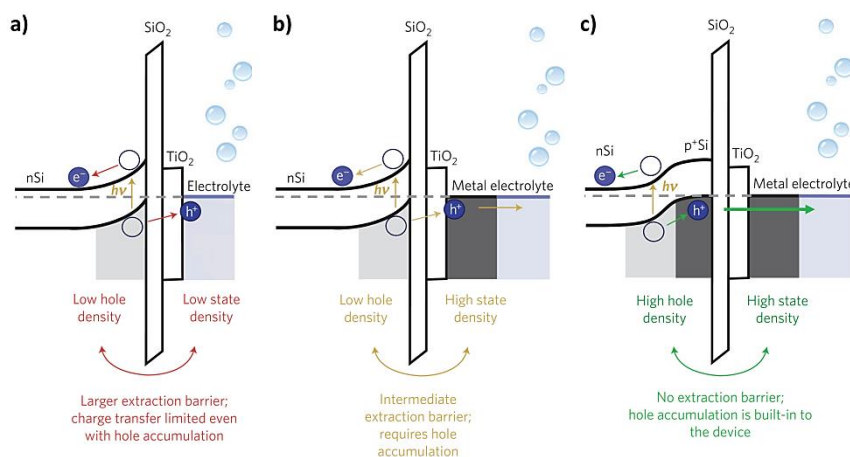


Figure 14. Three types of photoanode junctions have been employed in the ref. [156]: (a) semiconductor-liquid junction protected by SiO₂ and TiO₂, (b) MIS structure with metallic OEC, and (c) MIS with buried np⁺-junction. Here, the holes are transported via defect states of TiO₂. Reprinted with permission from ref. [156] Copyright 2016 Nature Publishing Group.

semiconductors; however they only investigated the mechanical degradation and did not focus on the electrical conduction through TiO₂. In 2011 Chen et al., used TiO₂ as a corrosion protection layer for a Si photoanode with a thin film of Ir as a catalyst.⁴⁴ The Chen work used an MIS structure to create photovoltage from their Si photoanode. They used the difference between the Fermi level in the n-Si and the Ir work function to induce band bending within the Si. The insulator in the MIS structure was a combination of a thin SiO₂ and the aforementioned TiO₂ protection layer. The authors hypothesized that charge was transferring through the TiO₂ via a trap assisted tunneling (Frenkel-Pool conduction)^{147,148} and in a later work showed a more detailed verification of this mechanism using various types of c-Si based photoanodes, including hybrid type MIS with buried pn⁺-junction (Fig. 14), which showed a photovoltage above 600 mV.¹⁵⁴

In the 2013 work by Seger et al.⁴³ where they showed TiO₂ as a cathodic protection layer, they also showed that it worked as a protection layer in an anodic environment.⁴³ While the anodic reactions in this work were H₂ oxidation, and oxidation of Fe²⁺ to Fe³⁺ the science discovered in this work provided the fundamental basis for further studies in anodic O₂ evolution (Fig. 15). There were three interesting discoveries from the Ref.⁴³: the first was that while pn⁺ Si electrodes have a band bending that favours electrons diffusing to the surface for reductive reactions, this work showed these types of electrodes can also achieve oxidative reactions. Simply put, the anodic charge coming from oxidized reactants at oxidative potentials would have occurred from band bending. The actual electrons that were oxidized from the reactants travelled through a TiO₂ and Ti layer into the Si conduction band where they recombined with holes in the silicon valence band. It should be noted that these holes were not primarily generated by photons, but rather valence band electrons that were extracted

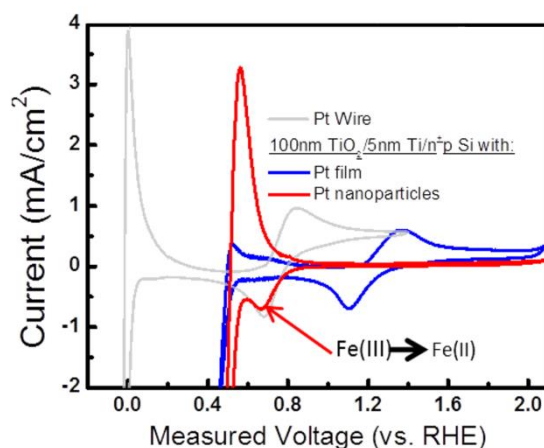


Figure 15. CV scans of a $\text{pn}^+\text{-Si/Ti/TiO}_2/\text{np-Pt}$ electrode in an argon-purged 1 M HClO_4 electrolyte with 10 mM each of Fe(III) and Fe(II) . The scan rate was 20 mV/s and the samples were irradiated with the red part ($\lambda > 635$ nm) of the AM1.5 spectrum. Reprinted with permission from Ref. 43. Copyright (YEAR) American Chemical Society

via the electrode (for use in the counter electrode). This allowed the device to maintain its photovoltage even as the oxidation reaction was occurring.

The second interesting issue is related to TiO_2 's band position. Given that TiO_2 's band position is near the H^+/H_2 redox couple, the authors showed that H_2 could be oxidized whereas band bending issues prevented $\text{Fe}^{2+}/\text{Fe}^{3+}$ oxidation (unless the TiO_2 was so highly doped it allowed for tunnelling).⁴⁷ However it was shown that the H_2 oxidation could continually occur even at potentials more oxidative than the $\text{Fe}^{2+}/\text{Fe}^{3+}$ redox couple. The fact that H_2 could oxidize at highly oxidative potentials, whereas Fe^{2+} could not, was attributed to the fact that the band bending within the TiO_2 caused a large potential drop within the semiconductor and that the actual oxidative potential of the TiO_2 at the semiconductor-electrolyte interface was only slightly more oxidative than the TiO_2 flat band potential.

The third interesting discovery from this work was the effects of sputtering a Pt film on top of the TiO_2 protected Si photoelectrode. In doing so, this completely isolated the TiO_2 from the electrolyte. This in turn eliminated any band bending due to the TiO_2 -electrolyte interface. However the TiO_2 -electrolyte interface was replaced by a TiO_2 -Pt interface, and it was unknown whether this would act as a Schottky barrier or an ohmic contact. When this Pt covered electrode was tested, it showed results similar to a Pt wire (except for the photovoltage shift) with the ability to both reduce Fe^{3+} and oxidize Fe^{2+} , thus indicating this was an ohmic contact. Typically the TiO_2 -Pt interface forms a Schottky-barrier, however the high dopant density of TiO_2 and the high energy of Pt sputtering into the TiO_2 could be potential reasons for this Ohmic contact. The practical results of these oxidation tests showed that one can basically bury a solar cell and 100 nm of TiO_2 , and it would behave equivalently as a solar cell in series with a conductive electrode. However this was only the case when

two very important parameters were met: 1) The semiconductor-electrolyte interface was removed and 2) TiO_2 -Pt formed an Ohmic contact.

With this in mind, it was straightforward to apply this principle to using TiO_2 as an anodic protection layer for O_2 evolution. After the Hu et al. work demonstrated that Leaky TiO_2 could be used as a photoanodic protection layer for O_2 evolution (*vide infra*), in the work by Mei et al. they used the same approach as in the Seger et al.⁴³ work, with this time using a $\text{p}^+\text{-Si}$ with a sputtered $\text{Ti/TiO}_2/\text{Pt}$ film, and they could indeed oxidize water to O_2 .⁵⁰ It should be noted that only sputtered Pt worked using this approach whereas evaporated Pt failed. This was hypothesized to be due to high energy impact from the sputtering process creating interfacial states thus allowing it to act more as an Ohmic contact rather than a Schottky barrier.^{150,151} This work also investigated the $\text{n}^+\text{Si/Ti}$ (or more probably $\text{n}^+\text{Si/TiSi}_x/\text{Ti}$)¹⁵² interface and showed both theoretically and experimentally that at high Si dopants levels charge could tunnel through the barrier created by the Si-TiSi_x Schottky barrier, whereas at low dopant densities charge could not tunnel through this barrier. This charge transport mechanism is well illustrated in Fig. 16.

While using a Pt film/ TiO_2 worked as an anodic protection layer, the Pt was actually interfacing with the electrolyte and was the primary protection layer. Creating a continuous film is an inefficient use of a catalytic material, especially one as expensive as Pt, but using nanoparticle catalyst will typically not work due to semiconductor band bending issues. However the intermediate case of small diameter islands of catalysts provides a very useful intermediate case. To understand how catalyst islands perform, one need to understand the fundamental concepts developed by Tung et al. and the work Robert Rossi and Nathan Lewis did applying this principle to mixed barrier heights at the semiconductor-electrolyte interface.^{153–155} In the Rossi and Lewis work they investigated the semiconductor/electrolyte interface of Si with evaporated Ni islands on the surface. In this situation there was a partial Si/electrolyte interface, which produced band bending, and a partial Si-Ni interface, which had a Schottky barrier. Through careful analysis they discussed the interaction between the semiconductor-electrolyte interface and the semiconductor-metal interface as a function of varying sizes of Ni islands. They showed that with very large Ni islands the Si/Ni interface behaved as a Schottky barrier, however as the size of the islands decreased, the effects of band bending from the Si/electrolyte interface actually started to creep in on the edges of the Ni islands. They showed that when Ni islands were below a certain diameter, the band bending would creep in from all sides and deep within the bulk the band bending potential

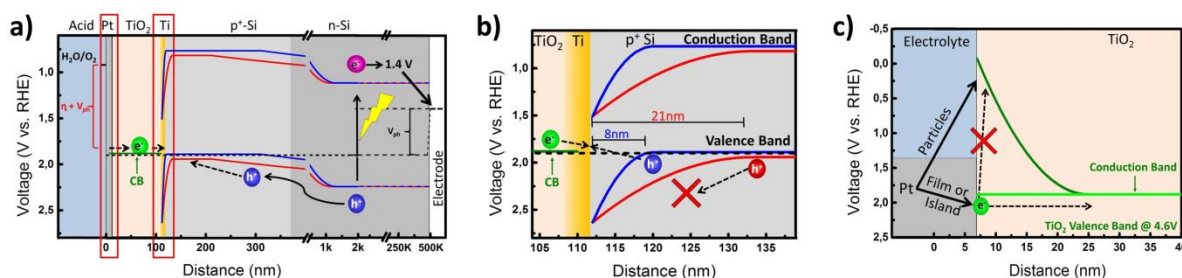


Figure 16. Band diagrams of an np⁺-Si/5 nm Ti/100 nm TiO₂/Pt Film Photoelectrode: (a) Overall band diagram at an applied Bias of 1.4 V versus RHE under Illumination; (b) Zoom in of the p⁺-Si/Ti Interface; (c) Zoom in of the TiO₂/Pt/electrolyte Interface from the overall band diagram shown in (a). Reproduced with permission from ref. [51]. Copyright (2015) American Chemical Society

would completely dominate, thus effectively ‘pinching-off’ the Schottky-barrier. Theoretical modeling allows one to determine the radius below which the pinch-off effect occurs as:

$$R_0 < \frac{(\Phi_{Elec} - \Phi_{Island})W}{V_{BB}} \quad \text{Eq. 1}$$

Where R_0 is the radius of the island, Φ_{Elec} and Φ_{Island} are the potential barrier between Si and the electrolyte and the island, respectively. W is the depletion width and V_{BB} is the voltage due to band bending.

The pinch-off effect is also very useful because it is a very straightforward explanation of why co-catalysts attached to photocatalysts almost never show any effects of a Schottky-barrier. Hill *et al.* has recently found a way to exploit this concept by using it to greatly enhance the photovoltage of n-Si-/Co interfaced devices.¹⁵⁶ In their work they showed that by electrodepositing Co islands they could pinch off the Si/Co electronic effects, and still use the dominant Si/electrolyte interface to achieve band bending and thus a high photovoltage. They followed this experiment up by showing that if the electrodeposited Co became a film this mitigated the Si-electrolyte interface and thus creating a Schottky barrier, which in turn, lowered the photovoltage.

On the other hand, however, Equation 1 shows that if the depletion width is small (as in the case of a highly doped semiconductor), the metal islands can actually be quite small and still maintain the electronic effects of the semiconductor-metal interface. This approach of creating small catalyst islands has been used in many instances including the aforementioned work by Mei *et al.*⁵⁰ Since the Mei work had already shown that a TiO₂/sputtered Pt film formed an Ohmic contact (see Fig. 16c), when they sputtered Pt catalyst islands on the TiO₂, the catalysts still maintained the Ohmic contact thus allowing for O₂ evolution to occur. Interestingly, the Pt nanoparticles (~5 nm) coated electrode case (Fig. 16c) showed a significant resistance in the Mei work⁵⁰ when it is used for OER, while there was no problems for the TiO₂ coated Si photocathodes which were coated

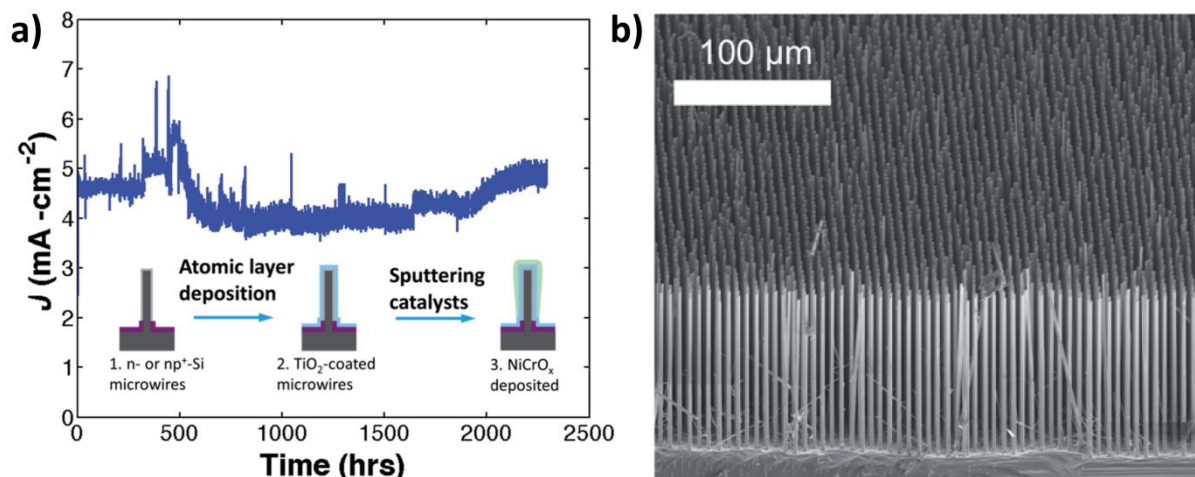


Figure 17. (a) CA for an np⁺-Si/TiO₂/NiCrO_x microwire-array photoelectrode under 1 Sun simulated illumination in 1.0 M KOH (pH 14) at 0.36 V vs. E(OH⁻/O₂). Schematic of a structure with fabrication procedure is added as inset. (b) SEM image of a fully processed microwire array. Reproduced by permission from Ref. [45] of The Royal Society of Chemistry.

by Pt nanoparticles with similar sizes.^{2,34,50,157} This can be explained by the aforementioned Schottky barrier at the Pt–TiO₂ due to the pinch-off effect.

Of recent works, the McIntyre group was the first to investigate TiO₂ as an O₂ evolution protection layer,⁴⁴ the Chorkendorff group was the first to investigate conduction through TiO₂ in anodic environments, but the Lewis group was the first to actually show conduction through thick (>10 nm) TiO₂ for photoanodic O₂ evolution. Additionally their method for transferring charge through the TiO₂ was much more ground breaking than the aforementioned approach used by the Chorkendorff group.

In the work by Hu et al., the Lewis group worked to create defect states throughout the an amorphous TiO₂ which they referred to as ‘Leaky TiO₂’.¹⁴ These defect states were located midway between the valence and conduction band and thus provided a path to allow charge to transfer at potentials near the O₂ evolution potential, as described earlier in chapter 2.2. This charge was then transferred to small catalytic islands on which O₂ was evolved. The semiconductor-catalyst interface appeared to be Ohmic for both evaporated and sputtered Ni, but there appeared to be significant resistance, possibly from a Schottky barrier when Ir was deposited. The Leaky TiO₂ has been shown to be effective on a wide variety of semiconductors such as planar and microwire Si, GaAs, GaP, CdTe.^{14,45,112} Particularly, a leaky TiO₂ protected NW np⁺-Si with NiCrO_x OEC layer demonstrated in Ref. ⁴⁵ has shown a record long-term stability in OER so far (Fig. 16). The ‘Leaky TiO₂’ was quite an unusual result, thus there were many questions regarding that. The 2016 follow up work by Hu et al. investigated the energy locations of the various states in a Si/leaky TiO₂ heterojunction and did a thorough job of investigating many of these questions.¹⁵⁸ Through a variety of techniques they showed a comprehensive

energy band diagram of the n-Si/leaky TiO₂ heterojunction with either a SiO₂ or Si_xTi_yO_z interface. They also showed that this n-Si/leaky TiO₂ could induce a 390 mV open circuit voltage. Man et al. investigated a very similar system using both n-Si/amorphous TiO₂ as well as p-Si/amorphous TiO₂ for photovoltaic applications.¹⁵⁹ In their study the TiO₂ did not act as a hole conducting layer, but rather a hole blocking layer. However they deposited TiO₂ via a CVD method at 100°C rather than an ALD at 150°C, which strongly hints that the exact deposition procedure is essential to create this Leaky TiO₂.

One of the more interesting follow up works on the Leaky TiO₂ was the work by McDowell et al, where they showed that a sputtered TiO₂ without significant mid gap defect states could also achieve anodic conductivity to evolve O₂.¹²¹ The McDowell et al. work by the Lewis group and the Mei et al work by the Chorkendorff group used the same sputtering TiO₂ technique for anodic conductivity, but unfortunately the both were published at almost the same time, thus neither of these works could mimic and compare to the other approach. However there are still some unresolved issues with Leaky TiO₂ such as exactly how charge conducts through the TiO₂. Both DFT calculations¹⁶⁰ and experimental results¹⁶¹ have shown that oxygen vacancies can allow for deep level trap sites as those found in the Leaky TiO₂. However calculations by Lewerenz show that the charge transfer was probably not due to a Poole-Frenkel type mechanism.¹⁶² While the Lewis group has shown amorphous 'Leaky' TiO₂ to be highly conductive to charge, the McIntyre's group has shown that their amorphous TiO₂ creates a barrier for conduction of charge.¹⁴⁸ While both their ALD processes appear quite similar, small difference must account for the discrepancies and further studies are needed to clarify this situation.

With the exception of the previously described Si-based photoanodes, very limited number of studies has reported meaningful OER stabilities in acidic solutions.^{14,131,134} Li et al. coated a thin IrO_x on the hematite (Fe₂O₃) photoanode and showed a stable PEC activity under OER conditions in adjusted HNO₃ with 0.1M KNO₃ (pH 1.01) for 5 hours. Although IrO_x coated Fe₂O₃ showed 5% photocurrent loss after the stability test, this is of significance because it was the first demonstration of OER using hematite in highly acidic solutions. Recently, Sarnowska et al.¹²⁹ also demonstrated stable OER in 1M CH₃SO₃H (pH ≈ 0) for 20 hours using sodium doped WO₃ without any co-catalyst and protection layer. However, as described above in the introduction part, the high E_g of WO₃ (~ 2.5 eV) fundamentally limits the light absorption and leads to poor photocurrent

performance ($\sim 3 \text{ mA cm}^{-2}$). On the other hand, this implies that n-WO₃ could potentially be used as a protection layer for highly acidic conditions rather than as a light absorber material.

4.3. Other layers

In general, tantalum oxynitride (TaON) has a sufficiently wide band-gap ($\sim 2.4 \text{ eV}$)¹⁶³ with suitable band alignment for both water oxidation and reduction, but it is also known to undergo deterioration in the highly oxidative environments, *e.g.*, under water oxidation condition by self-oxidation of nitrogen.¹⁶⁴ Higashi et al.¹⁶⁴ showed a modified TaON with IrO₂, which is an excellent OER catalyst, but it could maintain only 50% of the J_{int} in less than 10 min (@ 1.2V vs. RHE). Recently, Hou et al.¹⁶⁵ reported a non-metallic graphitic C₃N₄ coated 3D structured n-TaON with CoO_x co-catalyst that shows significantly enhanced photoelectrochemical stability (3 hours) under OER condition at pH 13.6 (1M NaOH). In addition, negative band offsets for both CB and VB (-1.0 eV and -0.5 eV , respectively) toward the TaON promote an effective charge separation for water oxidation reaction. 3D WO₃/C₃N₄ hetero-junctions decorated with nanoparticle CoO_x also exhibited enhanced PEC water oxidation performance and stability compared to the unprotected WO₃.¹⁶⁶ However, the efficiency of the TaON is limited by a wide band-gap that excludes photo-excitation by most of the solar spectrum leading to a maximum theoretical photocurrent of 7.5 mA cm^{-2} based on the Schottky-Queisser limit.¹⁶⁷

Carbon-based protection layers for high performance low band-gap photoanodes, *e.g.* Si, can be an appropriate example for comparison with other inorganic protection materials listed previously. Recently, Yoon et al.¹⁶⁸ coated n-type c-Si with a carbon-based protective multi-layer structure, which is composed of graphene-oxide (GO), single-walled carbon nanotubes, and graphene on top (*i.e.* n-Si/GO/SWCNT/Graphene) that showed stable water oxidation in 1M KOH (pH 14) for 15 min. This study revealed protection ability of CNT layer for n-Si photoanode for the first time, however, the origin of poor OER kinetics even at relatively high potential ($\sim 0.5 \text{ mA cm}^{-2}$ @ 1.4V vs. RHE) was not studied in detail.

5. Concluding remarks and outlooks

PEC stability and protection are critically important for the solar-fuel systems to be accepted as a reliable energy system, which can compete with other stability-proven renewable energy sources, such as PV and solar-thermal. Making tandem devices with stable oxide photocatalysts that have appropriate opto-electronic properties and options where this might not require protective layers (*e.g.*, Fe₂O₃, BiVO₄) in neutral pH can be a simple solution. However, as shown in the first chapter of this work, it is essential to have protective films

which can enable the use of technologically well-proven high-performing non-oxide solar cell materials, and development of robust protection thin films has become an emerging research field from early 2010 as demonstrated in Table S1, S2.

So far, various types of protection layer have been evaluated, and among them, TiO_2 has been proven for both photocathodes and photoanodes in a wide range of pH levels from acidic to alkaline, owing to its intrinsic chemical stability. Depending on operating conditions, the NiO_x -family can also be a promising candidate. Particularly, oxidation during OER activity makes the NiO_x a protective layer and efficient OEC layer in the high pH region. Self-enhancement in overpotential with iron-incorporation and simplicity in fabrication make this strategy attractive. In addition, recent developments with bi-polar membranes,¹⁶⁹ which can enable the operation of photocathode and photoanode at different pH conditions, increases degree of freedom in material selection for making full water splitting system.

In addition to this technological development in demonstration of the long-term stable PEC water splitting system, there have also been many scientific studies to understand the fundamentals of charge carrier transport, and to make more efficient PEC system. In this review we introduced representative carrier path mechanisms: electron transport via the conduction band (for photocathodes) and hole – via valence band (for photoanodes), tunneling via very thin insulating oxide, via defect states ('(defect) state-mediated transport' for photoanodes), and via hole-electron recombination at the photoanode/metal-oxide interface.

Despite significant progress, continued work on protection strategies for PEC systems is needed, particularly, the following aspects should be addressed for practical tandem PEC water splitting system: i) Stability and corrosion in the dark considering day/night operation in practical system; ii) Development of minimally damaging deposition processes for the sensitive PV materials, including, but not limited to organohalide perovskite semiconductors; iii) In-depth studies on new interfaces created by adding protection or other functional layer(s) for minimizing carrier-loss and maximizing photovoltage; iv) The dependency of OER kinetics on fabrication conditions.

Acknowledgements

The authors acknowledge the support of the support by VILLUM Center for Science of Sustainable Fuels and Chemicals which is funded from VILLUM Fonden research grant (9455).

[†]Supplementary information available: Supplementary dataset can be found in supporting information – parameters for ideal J-V curves in Figure 1; table S1 and S2.

- 1 S. Dahl and I. Chorkendorff, *Nat. Mater.*, 2012, **11**, 100–101.
- 2 D. Bae, T. Pedersen, B. Seger, M. Malizia, A. Kuznetsov, O. Hansen, I. Chorkendorff and P. C. K. Vesborg, *Energy Environ. Sci.*, 2015, **8**, 650–660.
- 3 M. G. Walter, E. L. Warren, J. R. Mckone, S. W. Boettcher, Q. Mi, E. A. Santori and N. S. Lewis, 2010, 6446–6473.
- 4 M. S. Burke, L. J. Enman, A. S. Batchellor, S. Zou and S. W. Boettcher, *Chem. Mater.*, 2015, **27**, 7549–7558.
- 5 K. Maeda, M. Higashi, D. Lu, R. Abe and K. Domen, *J. Am. Chem. Soc.*, 2010, **132**, 5858–5868.
- 6 T. Hisatomi, J. Kubota and K. Domen, *Chem. Soc. Rev.*, 2014, **43**, 7520–7535.
- 7 J. Hofkens and M. Roefaers, *Nature*, 2016, **530**, 36–37.
- 8 J. Rongé, T. Bosserez, D. Martel, C. Nervi, L. Boarino, F. Taulelle, G. Decher, S. Bordiga and J. A. Martens, *Chem. Soc. Rev.*, 2014, **43**, 7963–7981.
- 9 J. Jin, K. Walczak, M. R. Singh, C. Karp, N. S. Lewis and C. Xiang, *Energy Environ. Sci. Energy Environ. Sci.*, 2014, **7**, 3371–3371.
- 10 B. Seger, I. E. Castelli, P. C. K. Vesborg, K. W. Jacobsen, O. Hansen and I. Chorkendorff, *Energy Environ. Sci.*, 2014, **7**, 2397–2413.
- 11 R. van de Krol, *Photoelectrochemical Hydrogen Production in Electronic Materials: Science & Technology*, ed. R. van de Krol and M. Grätzel, Springer Science + Business Media, Boston, vol. 102, ch. 2, pp. 13–67.
- 12 H. S. Park, H. W. Ha, R. S. Ruoff and A. J. Bard, *J. Electroanal. Chem.*, 2014, **716**, 8–15.
- 13 M. G. Kast, L. J. Enman, N. J. Gurnon, A. Nadarajah and S. W. Boettcher, *ACS Appl. Mater. Interfaces*, 2014, **6**, 22830–22837.
- 14 S. Hu, M. R. Shaner, J. a Beardslee, M. Lichterman, B. S. Brunschwig and N. S. Lewis, *Science*, 2014, **344**, 1005–1009.
- 15 S. Hilaire, M. J. Suess, N. Kranzlin, K. Bienkowski, R. Solarska, J. Augustynski and M. Niederberger, *J. Mater. Chem. A*, 2014, **2**, 20530–20537.
- 16 C. G. Morales-Guio, S. D. Tilley, H. Vrubel, M. Grätzel and X. Hu, *Nat. Commun.*, 2014, **5**, 3059.
- 17 T. W. Kim and K.-S. K.-S. Choi, *Science (80-.)*, 2014, **343**, 990–994.
- 18 L. Zhang, T. Minegishi, M. Nakabayashi, Y. Suzuki, K. Seki, N. Shibata, J. Kubota and K. Domen, *Chem. Sci.*, 2015, **6**, 894–901.
- 19 A. Standing, S. Assali, L. Gao, M. A. Verheijen, D. van Dam, Y. Cui, P. H. L. Notten, J. E. M. Haverkort and E. P. A. M. Bakkers, *Nat. Commun.*, 2015, **6**, 7824.
- 20 Gurudayal, D. Sabba, M. H. Kumar, L. H. Wong, J. Barber, M. Grätzel and N. Mathews, *Nano Lett.*, 2015, **15**, 3833–3839.
- 21 K. Sun, Y. Kuang, E. Verlage, B. S. Brunschwig, C. W. Tu and N. S. Lewis, *Adv. Energy Mater.*, 2015, **5**, 1402276.
- 22 T. W. Kim, Y. Ping, G. A. Galli and K.-S. Choi, *Nat. Commun.*, 2015, **6**, 8769.
- 23 Y. Lin, R. Kapadia, J. Yang, M. Zheng, K. Chen, M. Hettick, X. Yin, C. Battaglia, I. D. Sharp, J. W. Ager and A. Javey, *J. Phys. Chem. C*, 2015, **119**, 2308–2313.
- 24 D. Bae, B. Mei, R. Frydendal, T. Pedersen, B. Seger, O. Hansen, P. C. K. Vesborg and I. Chorkendorff, *ChemElectroChem*, 2016, **3**, 1546–1552.
- 25 B. Seger, O. Hansen, P. C. K. Vesborg, *Sol. RRL*, 2016, 1600013.
- 26 M. M. May, H.-J. Lewerenz, D. Lackner, F. Dimroth and T. Hannappel, *Nat. Commun.*, 2015, **6**, 8286.
- 27 J. Y. Kim, G. Magesh, D. H. Youn, J.-W. Jang, J. Kubota, K. Domen and J. S. Lee, *Sci. Rep.*, 2013, **3**, 2681.
- 28 A. J. Bard, *J. Photochem.*, 1979, **10**, 59–75.
- 29 S. Chen and L.-W. Wang, *Chem. Mater.*, 2012, **24**, 3659–3666.
- 30 R. Liu, Z. Zheng, J. Spurgeon and X. Yang, *Energy Environ. Sci.*, 2014, **7**, 2504–2517.
- 31 O. Savadogo, *Sol. Energy Mater. Sol. Cells*, 1998, **52**, 361–388.
- 32 K. Walczak, Y. Chen, C. Karp, J. W. Beeman, M. Shaner, J. Spurgeon, I. D. Sharp, X. Amashukeli, W. West, J. Jin, N. S. Lewis and C. Xiang, *ChemSusChem*, 2015, **8**, 544–551.

- 33 N. Takeno, *Atlas of Eh-pH diagrams: Intercomposition of thermodynamics database*, National Institute of Advanced Industrial Science and Technology, Tokyo, 2005.
- 34 D. Bae, S. Shayestehaminzadeh, E. B. Thorsteinsson, T. Pedersen, O. Hansen, B. Seger, P. C. K. Vesborg, S. Ólafsson and I. Chorkendorff, *Sol. Energy Mater. Sol. Cells*, 2016, **144**, 758–765.
- 35 J. L. Young, K. X. Steirer, J. Dzara, Michael, J. A. Turner and T. G. Deutsch, *J. Mater. Chem. A*, 2016, **6**, 2831–2836.
- 36 A. Q. Contractor and J. O. Bockris, *Electrochim. Acta*, 1984, **29**, 1427–1434.
- 37 G. Li and S. Wang, *J. Electroanal. Chem. Interfacial Electrochem.*, 1987, **227**, 213–221.
- 38 B. Seger, A. B. Laursen, P. C. K. Vesborg, T. Pedersen, O. Hansen, S. Dahl and I. Chorkendorff, *Angew. Chemie - Int. Ed.*, 2012, **51**, 9128–9131.
- 39 P. A. Kohl, S. N. Frank and A. J. Bard, *J. Electrochem. Soc.*, 1977, **124**, 225–229.
- 40 A. Paracchino, V. Laporte, K. Sivula, M. Grätzel and E. Thimsen, *Nat. Mater.*, 2011, **10**, 456–461.
- 41 M. H. Lee, K. Takei, J. Zhang, R. Kapadia, M. Zheng, Y.-Z. Chen, J. Nah, T. S. Matthews, Y.-L. Chueh, J. W. Ager and A. Javey, *Angew. Chem. Int. Ed. Engl.*, 2012, **51**, 10760–10764.
- 42 B. Seger, S. D. Tilley, T. Pedersen, P. C. K. Vesborg, O. Hansen, M. Graetzel and I. Chorkendorff, *RSC Adv.*, 2013, **3**, 25902–25907.
- 43 B. Seger, T. Pedersen, A. B. Laursen, P. C. K. Vesborg, O. Hansen and I. Chorkendorff, *J. Am. Chem. Soc.*, 2013, **135**, 1057–1064.
- 44 Y. W. Chen, J. D. Prange, S. Dühnen, Y. Park, M. Gunji, C. E. D. Chidsey and P. C. McIntyre, *Nat. Mater.*, 2011, **10**, 539–544.
- 45 M. R. Shaner, S. Hu, K. Sun and N. S. Lewis, *Energy Environ. Sci.*, 2015, **8**, 203–207.
- 46 S. D. Tilley, M. Schreier, J. Azevedo, M. Stefik and M. Grätzel, *Adv. Funct. Mater.*, 2014, **24**, 303–311.
- 47 B. Seger, S. D. Tilley, T. Pedersen, P. C. K. Vesborg, O. Hansen, M. Graetzel and I. Chorkendorff, *J. Mater. Chem. a*, 2013, **1**, 15089–15094.
- 48 L. Ji, M. D. McDaniel, S. Wang, A. B. Posadas, X. Li, H. Huang, J. C. Lee, A. a Demkov, A. J. Bard, J. G. Ekerdt and E. T. Yu, *Nat. Nanotechnol.*, 2014, **10**, 84–90.
- 49 Z. W. Campet, G. Puprichitkun, C. and Sun, *J. Electroanal. Chem.*, 1989, **269**, 435–445.
- 50 B. Mei, T. Pedersen, P. Malacrida, D. Bae, R. Frydendal, O. Hansen, P. C. K. Vesborg, B. Seger and I. Chorkendorff, *J. Phys. Chem. C*, 2015, **119**, 15019–15027.
- 51 H. D. Abruna and A. J. Bard, *J. Am. Chem. Soc.*, 1981, **103**, 6898–6901.
- 52 A. Heller and R. G. Vadimsky, *Phys. Rev. Lett.*, 1981, **46**, 1153–1156.
- 53 A. Heller, E. Aharon-Shalom, W. A. Bonner and B. Miller, *J. Am. Chem. Soc.*, 1982, **104**, 6942–6948.
- 54 C. Maier, *Int. J. Hydrogen Energy*, 1996, **21**, 859–864.
- 55 B. Marsen, B. Cole and E. L. Miller, *Sol. Energy Mater. Sol. Cells*, 2008, **92**, 1054–1058.
- 56 D. Yokoyama, T. Minegishi, K. Maeda, M. Katayama, J. Kubota, A. Yamada, M. Konagai and K. Domen, *Electrochem. commun.*, 2010, **12**, 851–853.
- 57 Y. Hou, B. L. Abrams, P. C. K. Vesborg, M. E. Björketun, K. Herbst, L. Bech, A. M. Setti, C. D. Damsgaard, T. Pedersen, O. Hansen, J. Rossmeisl, S. Dahl, J. K. Nørskov and I. Chorkendorff, *Nat. Mater.*, 2011, **10**, 434–438.
- 58 A. Paracchino, N. Mathews, T. Hisatomi, M. Stefik, S. D. Tilley and M. Grätzel, *Energy Environ. Sci.*, 2012, **5**, 8673–8681.
- 59 E. L. Warren, J. R. McKone, H. a. Atwater, H. B. Gray and N. S. Lewis, *Energy Environ. Sci.*, 2012, **5**, 9653–9661.
- 60 J. Kim, T. Minegishi, J. Kobota and K. Domen, *Energy Environ. Sci.*, 2012, **5**, 6368–6374.
- 61 T. Bourgeteau, D. Tondelier, B. Geffroy, R. Brisse, C. Laberty-Robert, S. Campidelli, R. de Bettignies, V. Artero, S. Palacin and B. Joussetme, *Energy Environ. Sci.*, 2013, **6**, 2706–2713.
- 62 Z. Zhang, R. Dua, L. Zhang, H. Zhu, H. Zhang and P. Wang, *ACS Nano*, 2013, **7**, 1709–1717.
- 63 A. B. Laursen, T. Pedersen, P. Malacrida, B. Seger, O. Hansen, P. C. K. Vesborg and I. Chorkendorff, *Phys. Chem. Chem. Phys.*, 2013, **15**, 20000–20004.
- 64 Y. Lin, C. Battaglia, M. Boccard, M. Hettick, Z. Yu, C. Ballif, J. W. Ager and A. Javey, *Nano Lett.*, 2013, **13**, 5615–5618.
- 65 C.-Y. Lin, Y.-H. Lai, D. Mersch and E. Reisner, *Chem. Sci.*, 2012, **3**, 3482–3487.
- 66 Q. Ding, F. Meng, C. R. English, M. Cabán-Acevedo, M. J. Shearer, D. Liang, A. S. Daniel, R. J. Hamers and S. Jin, *J. Am. Chem. Soc.*, 2014, **136**, 8504–8507.
- 67 M. J. Choi, J.-Y. Jung, M.-J. Park, J.-W. Song, J.-H. Lee and J. H. Bang, *J. Mater. Chem. A*, 2014, **2**, 2928–2933.
- 68 L. Zhang, T. Minegishi, J. Kubota and K. Domen, *Phys. Chem. Chem. Phys.*, 2014, **16**, 6167–6174.

- 69 J. D. Benck, S. C. Lee, K. D. Fong, J. Kibsgaard, R. Sinclair and T. F. Jaramillo, *Adv. Energy Mater.*, 2014, **4**, 1400739.
- 70 C. Ros, T. Andreu, S. Giraldo, Y. Sánchez and J. R. Morante, *Sol. Energy Mater. Sol. Cells*, 2016, **158**, 184–188.
- 71 J. Feng, M. Gong, M. J. Kenney, J. Z. Wu, B. Zhang, Y. Li and H. Dai, *Nano Res.*, 2015, **8**, 1577–1583.
- 72 A. Azarpira, M. Lublow, A. Steigert, P. Bogdanoff, D. Greiner, C. A. Kaufmann, M. Krüger, U. Gernert, R. Van De Krol, A. Fischer and T. Schedel-Niedrig, *Adv. Energy Mater.*, 2015, **5**, 1402148.
- 73 R. Fan, W. Dong, L. Fang, F. Zheng, X. Su, S. Zou, J. Huang, X. Wang and M. Shen, *Appl. Phys. Lett.*, 2015, **106**, 13902.
- 74 H. Kumagai, T. Minegishi, N. Sato, T. Yamada, J. Kubota and K. Domen, *J. Mater. Chem. A*, 2015, **3**, 8300–8307.
- 75 I. A. Digdaya, P. P. Rodriguez, M. Ma, G. W. P. Adhyaksa, E. C. Garnett, A. H. M. Smets and W. A. Smith, *J. Mater. Chem. A*, 2016, **4**, 6842–6852.
- 76 M. Crespo-Quesada, L. M. Pazos-Outón, J. Warnan, M. F. Kuehnel, R. H. Friend and E. Reisner, *Nat. Commun.*, 2016, **7**, 12555.
- 77 Q. Li, M. Zheng, M. Zhong, L. Ma, F. Wang, L. Ma and W. Shen, *Sci. Rep.*, 2016, **6**, 29738.
- 78 F. Urbain, V. Smirnov, J.-P. Becker, A. Lambert, F. Yang, J. Ziegler, B. Kaiser, W. Jaegermann, U. Rau and F. Finger, *Energy Environ. Sci.*, 2016, **9**, 145–154.
- 79 J. Liang, H. Tan, M. Liu, B. Liu, N. Wang, Q. Zhang, Y. Zhao, A. H. M. Smets, M. Zeman and X. Zhang, *J. Mater. Chem. A*, 2016, **4**, 16841–16848.
- 80 J. Azevedo, S. D. Tilley, M. Schreier, M. Stefić, C. Sousa, J. P. Araújo, A. Mendes, M. Grätzel and M. T. Mayer, *Nano Energy*, 2016, **24**, 10–16.
- 81 R. J. Britto, J. D. Benck, J. L. Young, C. Hahn, T. G. Deutsch and T. F. Jaramillo, *J. Phys. Chem. Lett.*, 2016, **7**, 2044–2049.
- 82 D. Bae, T. Pedersen, B. Seger, B. Iandolo, O. Hansen, P. C. K. Vesborg and I. Chorkendorff, *Catal. Today*, 2016, DOI: 10.1016/j.cattod.2016.11.028.
- 83 O. Khaselev and J. A. Turner, *Electrochem. Solid-State Lett.*, 1999, **2**, 310–312.
- 84 J. R. McKone, A. P. Pieterick, H. B. Gray and N. S. Lewis, *J. Am. Chem. Soc.*, 2013, **135**, 223–231.
- 85 M. Malizia, B. Seger, I. Chorkendorff and P. C. K. Vesborg, *J. Mater. Chem. A*, 2014, **2**, 6847–6853.
- 86 E. D. Green, M. A. Emery, K.; Hishikawa, Y.; Warta, W.; Dunlop, *Prog. Photovolt Res. Appl.*, 2016, **24**, 905–913.
- 87 M. Grätzel, *Nature*, 1995, **414**, 338–344.
- 88 R. Fan, W. Dong, L. Fang, F. Zheng, X. Su, S. Zou, J. Huang, X. Wang and M. Shen, *Appl. Phys. Lett.*, 2015, **106**, 2–6.
- 89 J. R. Bakke, K. L. Pickrahn, T. P. Brennan and S. F. Bent, *Nanoscale*, 2011, **3**, 3482–3508.
- 90 W. M. Haynes, Ed., *CRC Handbook of Chemistry and Physics, 97th edition (Internet Version 2017)*, CRC Press/Taylor & Francis, Boca Raton, FL, 97th edn., 2016.
- 91 J. Feng, M. Gong, M. J. Kenney, J. Z. Wu, B. Zhang, Y. Li and H. Dai, *Nano Res.*, 2015, **1**, 1–4.
- 92 A. Azarpira, M. Lublow, A. Steigert, P. Bogdanoff, D. Greiner, C. A. Kaufmann, M. Krüger, U. Gernert, R. Van De Krol, A. Fischer and T. Schedel-Niedrig, *Adv. Energy Mater.*, 2015, **5**, 1–9.
- 93 E. Parzinger, B. Miller, B. Blaschke, J. A. Garrido, J. W. Ager, A. Holleitner and U. Wurstbauer, *ACS Nano*, 2015, **9**, 11302–11309.
- 94 J. D. Benck, T. R. Hellstern, J. Kibsgaard, P. Chakthranont and T. F. Jaramillo, *ACS Catal.*, 2014, **4**, 3957–3971.
- 95 P. C. K. Vesborg, B. Seger and I. Chorkendorff, *J. Phys. Chem. Lett.*, 2015, **6**, 951–957.
- 96 T. F. Jaramillo, K. P. Jørgensen, J. Bonde, J. H. Nielsen, S. Hørch and I. Chorkendorff, *Science*, 2007, **317**, 100–102.
- 97 B. Hinnemann, P. G. Moses, J. Bonde, K. P. Jørgensen, J. H. Nielsen, S. Hørch, I. Chorkendorff and J. K. Nørskov, *J. Am. Chem. Soc.*, 2005, **127**, 5308–5309.
- 98 D. Merki, S. Fierro, H. Vrubel and X. Hu, *Chem. Sci.*, 2011, **2**, 1262–1267.
- 99 A. G. Scheuermann and P. C. McIntyre, *J. Phys. Chem. Lett.*, 2016, **7**, 2867–2878.
- 100 R. C. Kainthla, *J. Electrochem. Soc.*, 1986, **133**, 248–253.
- 101 R. C. Kainthla, B. Zelenay and J. O. Bockris, *J. Electrochem. Soc.*, 1987, **134**, 841–845.
- 102 S. Y. Reece, J. a. Hamel, K. Sung, T. D. Jarvi, a. J. Esswein, J. J. H. Pijpers and D. G. Nocera, *Science (80-.)*, 2011, **334**, 645–648.
- 103 M. Liao, J. Feng, W. Luo, Z. Wang, J. Zhang, Z. Li, T. Yu and Z. Zou, *Adv. Funct. Mater.*, 2012, **22**, 3066–3074.

- 104 K. Sun, N. Park, Z. Sun, J. Zhou, J. Wang, X. Pang, S. Shen, S. Y. Noh, Y. Jing, S. Jin, P. K. L. Yu and D. Wang, *Energy Environ. Sci.*, 2012, **5**, 7872–7877.
- 105 M. J. Kenney, M. Gong, Y. Li, J. Z. Wu, J. Feng, M. Lanza and H. Dai, *Science* (80-.), 2013, **342**, 836–840.
- 106 M. F. Lichtenman, M. R. Shaner, S. G. Handler, B. S. Brunschwig, H. B. Gray, N. S. Lewis and J. M. Spurgeon, *J. Phys. Chem. Lett.*, 2013, **4**, 4188–4191.
- 107 N. C. Strandwitz, D. J. Comstock, R. L. Grimm, A. C. Nichols-Nieler, J. Elam and N. S. Lewis, *J. Phys. Chem. C*, 2013, **117**, 4931–4936.
- 108 M. Higashi, K. Domen and R. Abe, *J. Am. Chem. Soc.*, 2013, **135**, 10238–10241.
- 109 K. Sun, X. Pang, S. Shen, X. Qian, J. S. Cheung and D. Wang, *Nano Lett.*, 2013, **13**, 2064–2072.
- 110 B. Mei, A. a Permyakova, R. Frydendal, D. Bae, T. Pedersen, P. Malacrida, O. Hansen, I. E. L. Stephens, P. C. K. Vesborg, B. Seger and I. Chorkendor, *J. Phys. Chem. Lett.*, 2014, **5**, 3456–3461.
- 111 J. Yang, K. Walczak, E. Anzenberg, F. M. Toma, G. Yuan, J. Beeman, A. Schwartzberg, Y. Lin, M. Hettick, A. Javey, J. W. Ager, J. Yano, H. Frei and I. D. Sharp, *J. Am. Chem. Soc.*, 2014, **136**, 6191–6194.
- 112 M. F. Lichtenman, A. I. Carim, M. T. McDowell, S. Hu, H. B. Gray, B. S. Brunschwig and N. S. Lewis, *Energy Environ. Sci.*, 2014, **7**, 3334–3337.
- 113 G. Liu, J. Shi, F. Zhang, Z. Chen, J. Han, C. Ding, S. Chen, Z. Wang, H. Han and C. Li, *Angew. Chemie - Int. Ed.*, 2014, **53**, 7295–7299.
- 114 M. T. McDowell, M. F. Lichtenman, J. M. Spurgeon, S. Hu, I. D. Sharp, B. S. Brunschwig and N. S. Lewis, *J. Phys. Chem. C*, 2014, **118**, 19618–19624.
- 115 K. Sun, S. Shen, J. S. Cheung, X. Pang, N. Park, J. Zhou, Y. Hu, Z. Sun, S. Y. Noh, C. T. Riley, P. K. L. Yu, S. Jin and D. Wang, *Phys. Chem. Chem. Phys.*, 2014, **16**, 4612–25.
- 116 E. S. Kim, H. J. Kang, G. Magesh, J. Y. Kim, J. W. Jang and J. S. Lee, *ACS Appl. Mater. Interfaces*, 2014, **6**, 17762–17769.
- 117 B. Mei, B. Seger, T. Pedersen, M. Malizia, O. Hansen, I. Chorkendorff and P. C. K. Vesborg, *J. Phys. Chem. Lett.*, 2014, **5**, 1948–1952.
- 118 X. Shi, I. Y. Choi, K. Zhang, J. Kwon, D. Y. Kim, J. K. Lee, S. H. Oh, J. K. Kim and J. H. Park, *Nat. Commun.*, 2014, **5**, 4775.
- 119 K. Sun, M. T. McDowell, A. C. Nieler, S. Hu, M. R. Shaner, F. Yang, B. S. Brunschwig and N. S. Lewis, *J. Phys. Chem. Lett.*, 2015, **6**, 592–598.
- 120 K. Sun, F. H. Saadi, M. F. Lichtenman, W. G. Hale, H.-P. Wang, X. Zhou, N. T. Plymale, S. T. Omelchenko, J.-H. He, K. M. Papadantonakis, B. S. Brunschwig and N. S. Lewis, *Proc. Natl. Acad. Sci.*, 2015, **112**, 3612–3617.
- 121 M. T. McDowell, M. F. Lichtenman, A. I. Carim, R. Liu, S. Hu, B. S. Brunschwig and N. S. Lewis, *ACS Appl. Mater. Interfaces*, 2015, **7**, 15189–15199.
- 122 X. Zhou, R. Liu, K. Sun, D. Friedrich, M. T. McDowell, F. Yang, S. T. Omelchenko, F. H. Saadi, A. C. Nieler, S. Yalamanchili, K. M. Papadantonakis, B. S. Brunschwig and N. Lewis, *Energy Environ. Sci.*, 2015, **8**, 2644–2649.
- 123 L. Chen, J. Yang, S. Klaus, L. J. Lee, R. Woods-Robinson, J. Ma, Y. Lum, J. K. Cooper, F. M. Toma, L. W. Wang, I. D. Sharp, A. T. Bell and J. W. Ager, *J. Am. Chem. Soc.*, 2015, **137**, 9595–9603.
- 124 C. Li, T. Wang, Z. Luo, D. Zhang and J. Gong, *Chem. Commun.*, 2015, **51**, 7290–7293.
- 125 M. Zhong, T. Hisatomi, Y. Kuang, J. Zhao, M. Liu, A. Iwase, Q. Jia, H. Nishiyama, T. Minegishi, M. Nakabayashi, N. Shibata, R. Niishiro, C. Katayama, H. Shibano, M. Katayama, A. Kudo, T. Yamada and K. Domen, *J. Am. Chem. Soc.*, 2015, **137**, 5053–5060.
- 126 W. Li, S. W. Sheehan, D. He, Y. He, X. Yao, R. L. Grimm, G. W. Brudvig and D. Wang, *Angew. Chemie - Int. Ed.*, 2015, **54**, 11428–11432.
- 127 J. H. Kim, Y. Jo, J. H. Kim, J. W. Jang, H. J. Kang, Y. H. Lee, D. S. Kim, Y. Jun, J. S. Lee and K. I. M. E. T. Al, *ACS Nano*, 2015, **9**, 11820–11829.
- 128 I. Narkeviciute, P. Chakthranont, A. J. M. Mackus, C. Hahn, B. A. Pinaud, S. F. Bent and T. F. Jaramillo, *Nano Lett.*, 2016, **16**, 7565–7572.
- 129 M. Sarnowska, K. Bienkowski, P. J. Barczuk, R. Solarska and J. Augustynski, *Adv. Energy Mater.*, 2016, **6**, 1–6.
- 130 S. Akiyama, M. Nakabayashi, N. Shibata, T. Minegishi, Y. Asakura, M. Abdulla -Al-Mamun, T. Hisatomi, H. Nishiyama, M. Katayama, T. Yamada and K. Domen, *Small*, 2016, **12**, 5468–5476.
- 131 W. L. Kwong, C. C. Lee and J. Messinger, *J. Phys. Chem. C*, 2016, **120**, 10941–10950.
- 132 T. Yao, R. Chen, J. Li, J. Han, W. Qin, H. Wang, J. Shi, F. Fan and C. Li, *J. Am. Chem. Soc.*, 2016, **138**, 13664–13672.
- 133 E. S. Kim, N. Nishimura, G. Magesh, J. Y. Kim, J. Jang, H. Jun, J. Kubota, K. Domen and J. S. Lee, *J. Am.*

- Chem. Soc., 2013, **135**, 5375–5383.
- 134 J. M. Spurgeon, J. M. Velazquez and M. T. McDowell, *Phys. Chem. Chem. Phys.*, 2014, **16**, 3623–3631.
- 135 S. Cherevko, S. Geiger, O. Kasian, N. Kulyk, J. P. Grote, A. Savan, B. R. Shrestha, S. Merzlikin, B. Breitbach, A. Ludwig and K. J. J. Mayrhofer, *Catal. Today*, 2016, **262**, 170–180.
- 136 S. Bai, M. Cao, Y. Jin, X. Dai, X. Liang, Z. Ye, M. Li, J. Cheng, X. Xiao, Z. Wu, Z. Xia, B. Sun, E. Wang, Y. Mo, F. Gao and F. Zhang, *Adv. Energy Mater.*, 2014, **4**, 1–6.
- 137 M. D. Irwin, D. B. Buchholz, A. W. Hains, R. P. H. Chang and T. J. Marks, *Proc. Natl. Acad. Sci.*, 2008, **105**, 2783–2787.
- 138 E. Nurlaela, H. Wang, T. Shinagawa, S. Flanagan, S. Ould-Chikh, M. Qureshi, Z. Mics, P. Sautet, T. Le Bahers, E. Cánovas, M. Bonn and K. Takanabe, *ACS Catal.*, 2016, **6**, 4117–4126.
- 139 L. Trotochaud, S. L. Young, J. K. Ranney and S. W. Boettcher, *J. Am. Chem. Soc.*, 2014, **136**, 6744–6753.
- 140 M. S. Burke, M. G. Kast, L. Trotochaud, A. M. Smith and S. W. Boettcher, *J. Am. Chem. Soc.*, 2015, **137**, 3638–3648.
- 141 G. Li and S. Wang, *J. Electroanal. Chem. Interfacial Electrochem.*, 1987, **227**, 213–221.
- 142 H. Sato, T. Minami, S. Takata and T. Yamada, *Thin Solid Films*, 1993, **236**, 27–31.
- 143 B. A. Nail, J. M. Fields, J. Zhao, J. Wang, M. J. Greaney, R. L. Brutchey and F. E. Osterloh, *ACS Nano*, 2015, 5135–5142.
- 144 Y. Jiang, X. Li, T. Wang and C. Wang, *Nanoscale*, 2016, 9667–9675.
- 145 C.-W. Tung, Y.-Y. Hsu, Y.-P. Shen, Y. Zheng, T.-S. Chan, H.-S. Sheu, Y.-C. Cheng and H. M. Chen, *Nat. Commun.*, 2015, **6**, 8106.
- 146 M. Tomkiewicz and J. M. Woodall, *J. Electrochem. Soc.*, 1977, **124**, 1436.
- 147 J. Nelson and R. E. Chandler, *Coord. Chem. Rev.*, 2004, **248**, 1181–1194.
- 148 A. G. Scheuermann, J. D. Prange, M. Gunji, C. E. D. Chidsey and P. C. McIntyre, *Energy Environ. Sci.*, 2013, **6**, 2487–2496.
- 149 A. G. Scheuermann, J. P. Lawrence, K. W. Kemp, T. Ito, A. Walsh, C. E. D. Chidsey, P. K. Hurley and P. C. McIntyre, *Nat. Mater.*, 2016, **15**, 99–105.
- 150 U. K. Kirner, K. D. Schierbaum and W. Göpel, *Fresenius. J. Anal. Chem.*, 1991, **341**, 416–420.
- 151 M. Cerchez, H. Langer, M. El Achhab, T. Heinzl, D. Ostermann, H. Lüder and J. Degenhardt, *Appl. Phys. Lett.*, 2013, **103**, 033522.
- 152 W. De Bosscher, R. Van Meirhaeghe, A. De Laere, W. Laflere and F. Cardon, *Solid. State. Electron.*, 1988, **31**, 1629–1634.
- 153 R. T. Tung, *Appl. Phys. Lett.*, 1991, **58**, 2821–2823.
- 154 R. T. Tung, *Phys. Rev. B*, 1992, **45**, 13509–13523.
- 155 R. C. Rossi and N. S. Lewis, *J. Phys. Chem. B*, 2001, **105**, 12303–12318.
- 156 J. C. Hill, A. T. Landers and J. a Switzer, *Nat Mater*, 2015, **14**, 1150–1155.
- 157 E. Kemppainen, A. Bodin, B. Sebok, T. Pedersen, B. Seger, B. Mei, D. Bae, P. C. K. Vesborg, J. Halme, O. Hansen, P. D. Lund and I. Chorkendorff, *Energy Environ. Sci.*, 2015, **8**, 2991–2999.
- 158 S. Hu, M. H. Richter, M. F. Lichterman, J. Beardslee, T. Mayer, B. S. Brunshwig and N. S. Lewis, *J. Phys. Chem. C*, 2016, **120**, 3117–3129.
- 159 G. Man, J. Schwartz, J. C. Sturm and A. Kahn, *Adv. Mater. Interfaces*, 2016, **3**, 1–8.
- 160 H. H. Pham and L.-W. Wang, *Phys. Chem. Chem. Phys.*, 2015, **17**, 541–550.
- 161 P. Reckers, M. Dimamay, J. Klett, S. Trost, K. Zilberberg, T. Riedl, B. A. Parkinson, J. Brötz, W. Jaegermann and T. Mayer, *J. Phys. Chem. C*, 2015, **119**, 9890–9898.
- 162 H. J. Lewerenz, *J. Electrochem. Soc.*, 2014, **161**, H3117–H3129.
- 163 W. Chun, A. Ishikawa, H. Fujisawa, T. Takata, J. N. Kondo, M. Hara, M. Kawai, Y. Matsumoto and K. Domen, *J. Phys. Chem. B*, 2003, **107**, 1798–1803.
- 164 M. Higashi, K. Domen and R. Abe, *J. Am. Chem. Soc.*, 2012, **134**, 6968–6971.
- 165 J. Hou, H. Cheng, O. Takeda and H. Zhu, *Energy Environ. Sci.*, 2015, **8**, 1348–1357.
- 166 Y. Hou, F. Zuo, A. P. Dagg, J. Liu and P. Feng, *Adv. Mater.*, 2014, **26**, 5043–5049.
- 167 W. Shockley and H. J. Queisser, *J. Appl. Phys.*, 1961, **32**, 510–519.
- 168 K. Yoon, J.-H. Lee, J. Kang, J. Kang, M. J. Moody, M. C. Hersam and L. J. Lauhon, *Nano Lett.*, 2016, **16**, 7370–7375.
- 169 J. Luo, D. A. Vermaas, D. Bi, A. Hagfeldt, W. A. Smith, M. Grätzel, *Adv. Energy Mater.*, 2016, **6**, 1600100.

Dowon Bae received his BSc. and MSc. (Honors) from Russian State Technological University named after K.E. Tsiolkovsky in 2006 and 2008, respectively. After the research activities in Cu(In,Ga)Se₂ solar cell at the LG Innotek, he joined the Danish National Research Foundation “*CINF*” (Center for Individual Nanoparticle Functionality) at the Technical University of Denmark (DTU), where he completed his PhD in 2012 under supervision by Prof. Ib Chorkendorff. Presently, he is a postdoctoral researcher of the VILLUM Center for the Science of Sustainable Fuels and Chemicals at the DTU Physics. His research concerns PEC device design and fabrication for solar-fuel production.

Prof. Brian Seger completed his Ph.D. from Notre Dame under Prof. Prashant Kamat in 2009. He has since completed postdocs at the University of Queensland under Lian Zhou Wang and he joined the “*CINF*” at DTU under Prof. Ib Chorkendorff. Since 2014, he has been an assistant professor at DTU Physics. His research interests include understanding semiconductor-electrolyte interfaces, discovering new photoactive materials, and modeling photoelectrochemical devices.

Peter C. K. Vesborg received his Ph.D. degree in Applied Physics from the DTU in 2010. He then went to the department of Chemical Engineering at Stanford University as a postdoc under Prof. Thomas Jaramillo before returning to DTU to join the faculty of the department of Physics in 2012, where he has been associate professor since 2015. His research concerns catalysis (thermal, electro-, and photocatalysis), photoelectrodes, MEMS-based device development for catalyst benchmarking, and global resource availability and management for sustainable technologies.

Prof. Ole Hansen received the MSc. degree in micro-technology from the DTU in 1977. Since 1977 he has worked with micro- and nano-technology and applications of the technology within electronics, metrology, sensing, catalysis and energy harvesting. Currently, he is Professor at DTU Nanotech, where he is heading the Silicon Microtechnology group. Current research interests include sustainable energy, photocatalysis and tools for characterizing catalytic processes. From 2005-2016 he was part of the ‘*CINF*’, and presently, he is part of ‘*V-SUSTAIN*’ (VILLUM Center for the Science of Sustainable Fuels and Chemicals).

Prof. Ib Chorkendorff got his PhD from Odense University (1985). After working as a post-doc with Prof. John T. Yates Jr. at University of Pittsburgh, he was employed at DTU (1987) to establish an experimental activity, investigating fundamental aspects of heterogeneous catalysis. He was Director of the ‘*CINF*’ (2005-2016) and subsequent Director of the ‘*V-SUSTAIN*’. He has been author of close to 300 scientific papers and 17 patents. His research activities focus on surface reactions and finding new materials to improve energy production/conversion and environmental protection. He is co-founder of start-up companies RENCAT APS, HPNOW APS and Spectroinlets APS.

This review provides a comprehensive overview of the key aspects of protection strategies for achieving stable solid/liquid interfaces for photoelectrodes.

